

Biologically-inspired selective filters

by

Laura K. Maguire

B.S., Harvey Mudd College, 2013

A thesis submitted to the
Faculty of the Graduate School of the
University of Colorado in partial fulfillment
of the requirements for the degree of
Doctor of Philosophy
Department of Physics
2019

This thesis entitled:
Biologically-inspired selective filters
written by Laura K. Maguire
has been approved for the Department of Physics

Assistant Professor Loren Hough

Professor Attendant Rank Matthew Glaser

Date _____

The final copy of this thesis has been examined by the signatories, and we find that both the content and the form meet acceptable presentation standards of scholarly work in the above mentioned discipline.

Maguire, Laura K. (Ph.D., Physics)

Biologically-inspired selective filters

Thesis directed by Assistant Professor Loren Hough

Selective biofilters are essential to life, controlling the transport of proteins, nucleic acids, and other macromolecules. Of particular interest are filters which require rapid motion or high flux of proteins that must still bind targets with high specificity. Despite the apparent competition between these two attributes, many selective materials exist which leverage binding interactions to fulfill both. In this work, we investigate the mechanisms by which such filters function through both modeling and experiment, using the nuclear pore, a well-studied example of selective transport, as inspiration. The nuclear pore, a channel lined with intrinsically disordered FG nucleoporins, permits a high flux of transport factor proteins and their cargos while suppressing transport of proteins which cannot bind to the FG nucleoporins. We developed a minimal model of nuclear transport which relies on the bound-state mobility of the Nup-transport factor complex for selectivity. This model reproduces the experimentally-observed properties of the nuclear pore and demonstrates that bound-state diffusion can arise from transient, multivalent binding and binding to flexible, dynamic tethers. We then designed tunable hydrogel mimics of the nuclear pore for use in measuring bound-state diffusion and testing the predictions of our model. Fluorescence microscopy demonstrated that our mimics display non-zero bound diffusion. Both the model and experimental system are sufficiently general that their principles can be applied to a wide variety of selective biomaterials.

Contents

Chapter

1	Introduction	1
1.1	The nuclear pore complex is a unique selective filter	1
1.1.1	Intrinsically disordered proteins	2
1.1.2	Basics of nuclear transport	3
1.1.3	Models of nuclear transport	7
1.1.4	Nuclear pore mimics	10
1.2	Other selective biofilters	12
1.2.1	Drug delivery through mucus barriers	13
1.2.2	Diffusion of DNA-binding proteins in the nucleus	14
1.2.3	Subcompartments in liquid droplets	16
1.3	Project goals and motivation	17
1.3.1	Minimal model of selective transport	18
1.3.2	Experimental tests of bound-state diffusion in biomaterials	19
1.4	Biophysics is beautiful	21
2	FG Nup aggregation under crowded conditions	23
2.1	Fluorescence time courses	26
2.1.1	Methods	28
2.1.2	Results	30

2.1.3	Discussion	32
2.2	Fluorescence spectra	34
2.2.1	Methods	35
2.2.2	Results	36
2.2.3	Discussion	37
2.3	NMR relaxation measurements	39
2.3.1	Methods	40
2.3.2	Results	41
2.3.3	Discussion	42
2.4	Conclusions	43
3	Conclusions and future directions	44
3.1	Future directions	45
Bibliography		48
Appendix		

Tables

Table

2.1	Aggregation rates and lag times for all crowding agents.	31
2.2	Aggregation lifetimes and lag times with varying pH.	32

Figures

Figure

1.1	Nuclear pore complex and FG Nups.	4
1.2	Two important models of nuclear transport.	8
1.3	Effective-potential model of nuclear transport.	9
1.4	Nanoparticle drug delivery through a mucus barrier.	13
1.5	Phase-separated subcompartments of the nucleolus.	16
2.1	Aggregation of FG Nups into amyloid fibrils.	24
2.2	Sample sigmoid fit to FG124 aggregation timecourse.	27
2.3	Aggregation rates and lag times for all crowding agents.	31
2.4	Aggregation rates and lag times for varying PEG and PVP concentrations.	33
2.5	Chemical structures of PEG and PVP.	35
2.6	Fluorescence and absorbance of crowders.	36
2.7	Fluorescence spectra of FSFG, FG124, and phenylalanine.	37
2.8	FG124 fluorescence in crowded conditions.	38
2.9	FG124 fluorescence comparison between crowding agents.	38
2.10	Classes of tryptophan fluorescence.	39
2.11	Relaxation times of FSFG in crowded conditions.	41
2.12	Approximate dependence of relaxation times on viscosity.	42

Chapter 1

Introduction

Selective biofilters are found in all manner of living systems and control the motion of proteins, nucleic acids, and other macromolecules. While many operate by size exclusion, permitting only the passage of particles below a size cutoff, more sophisticated filters make use of binding interactions. Of particular interest are filters which require rapid motion or high flux of proteins that must still bind targets with high specificity. The two requirements would seem to be in direct competition, yet there are many examples of these systems. In this work, we investigate the mechanisms by which such filters function through both modeling and experiment, using the nuclear pore, a canonical example of selective transport, as inspiration.

1.1 The nuclear pore complex is a unique selective filter

The nuclear pore complex (NPC) is the filter that regulates all transport between the cell's nucleus and its cytoplasm (Fig. 1.1). It shows unusual selective properties. The nuclear pore prevents significant flux of macromolecules larger than about 30 kDa (~ 5 nm) [1]. However, a class of proteins known as transport factors carry cargo molecules quite rapidly across the pore, although the complex of transport factor and cargo can be up to 40 nm in size. Far from being a typical size-exclusion filter, therefore, the nuclear pore complex is a highly specific selective barrier which the cell uses to tightly control passage in and out of the nucleus. While the important biochemical components of nuclear transport have been identified, the mechanism of selectivity is

still not well understood. Even though the precise mechanism is under debate, it is clear that the NPC is a fascinating example of the cell leveraging intrinsically disordered proteins to accomplish a unique task.

1.1.1 **Intrinsically disordered proteins**

It has been long-standing conventional wisdom among biologists that a protein's folded shape determines its function. Most enzymes and other proteins that were studied had a stable folded configuration, the lowest point on a well-defined folding energy landscape. A protein's conformation provided specific docking points through which it could interact with ligands or other proteins in a "lock-and-key" model.

However, a few decades ago, it began to become clear that not all proteins have a well-defined ternary or even secondary structure, but rather exist as extended polymer chains. These intrinsically disordered proteins (IDPs) were initially dismissed as nonfunctional, but evidence began to accumulate that they were in fact essential for cellular function, modifying the structure-function paradigm. Their roles and importance are still being understood, as are the unusual mechanisms by which they accomplish their functions without a well-defined structure.

Today, it is estimated that 30% of eukaryotic proteins are disordered or contain significant disordered regions [2]. While there is significant sequence heterogeneity among IDPs, they tend to contain a large proportion of hydrophilic residues, and often have long stretches of low-complexity regions where only a few amino acids are represented. They also often have high net charge.

Some IDPs fold (or partially fold) upon binding with an ordered partner, while others form a "fuzzy" complex that remains disordered. Their advantages over folded proteins may include their plasticity, which enables them to bind many different binding partners. Multivalency, either as one-to-many or many-to-one binding, may also play a role. They may act as hubs that bring together larger complexes. Similarly, IDPs are often known for having high specificity at relatively weak binding strengths [3, 4].

While the normal functioning of IDPs is important to the cell, IDPs are also prone to aggre-

gation and are at the root of pathologies such as Alzheimer's, Parkinson's, and prion diseases [5]. Often, normally-disordered proteins aggregate into amyloid fibrils, a stable structure consisting of stacked β -sheets.

IDPs are commonly involved in cell signaling and regulation [3]. Their disordered nature makes them useful as hubs that bring together many other proteins, and as scaffolds that many proteins can bind to at once. IDPs appear to be prevalent in transcriptional regulation, and they are playing increasingly apparent roles in liquid-liquid phase separation within cells [6]. One of the most fascinating examples of IDP function is in the nuclear pore complex (NPC), a unique selective barrier that regulates all transport between the nucleus and the cytoplasm. The link between disorder and selectivity is not well understood in this case.

1.1.2 Basics of nuclear transport

The nuclear pore complex (NPC) resides in the nuclear envelope of eukaryotes and regulates all macromolecular traffic between the nucleus and cytoplasm (Fig. 1.1). The NPC is one of the largest protein complexes in the cell, at about 60 MDa in yeast and 120 MDa in humans [7]. As the regulator of nucleocytoplastic transport, the NPC must rapidly and specifically allow the passage of a wide array of macromolecules: transcription factors into the nucleus, and RNA into the cytoplasm. It must also be robust to perturbations and able to accommodate mechanical strain as the nuclear envelope changes shape, as well as during the passage of large cargo. These functions are accomplished through a structure with two major components, both made of proteins known as nucleoporins, or Nups: the scaffold Nups, which form a ringlike complex, and the FG Nups, which are disordered and fill the central channel created by the scaffold Nups (Fig. 1.1).

The nuclear pore itself is formed of scaffold Nups, which are ordered proteins that form ring structures with eightfold symmetry [7,9]. The central channel of the pore is filled with disordered FG Nups. FG Nups typically consist of an ordered domain that anchors them to the wall of the channel and an entirely disordered domain that extends into the channel. As with all Nups, FG Nups have eightfold symmetry in the pore, and some of them are present in much higher copy number. The

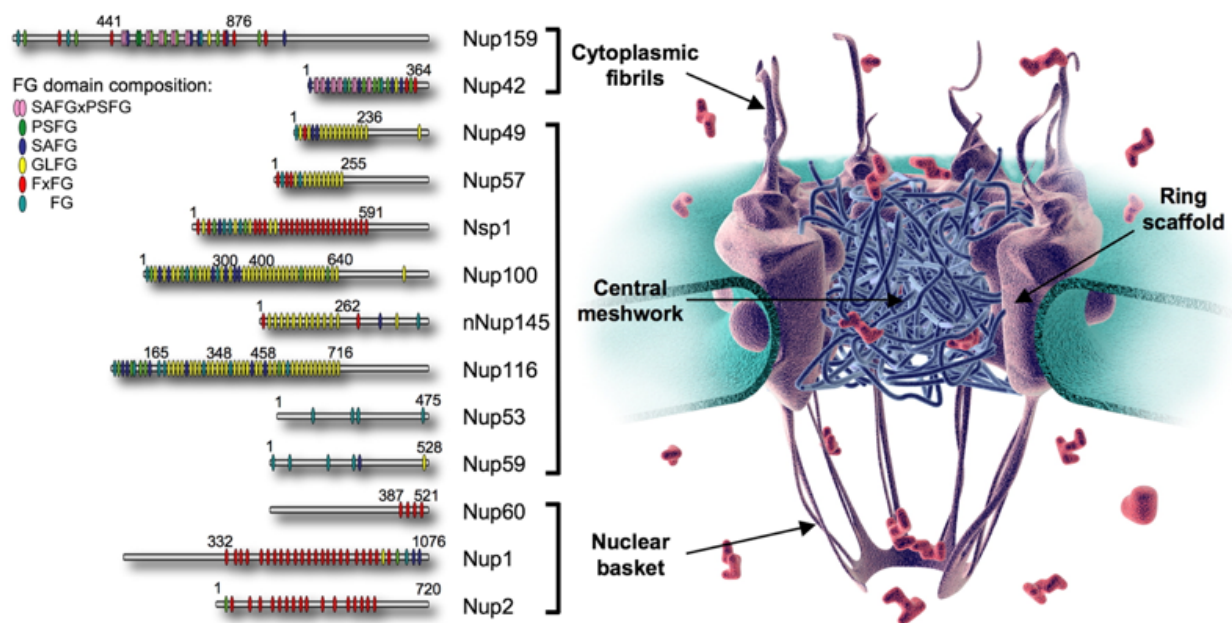


Figure 1.1: Nuclear pore complex and FG Nups. The cartoon shows the role of the FG Nups filling the central channel. The left panel shows a schematic of the sequences of important FG Nups and the locations of their FG motifs. Figure adapted from [8].

disordered portion of every FG Nup contains phenylalanine- glycine (FG) motifs which bind to the hydrophobic binding pockets of transport factors. While there are multiple binding motifs, all are short sequences which incorporate an FG repeat; for instance, FSFG, GLFG, and others. Each FG Nup contains tens of FG repeats, leading to a high density of FG repeats within the pore [9, 10].

Since the FG Nups are disordered, most conventional visualization techniques, such as cryogenic electron microscopy and x-ray crystallography, are ineffective. When imaged over time or when several pores are imaged, the averaged results do not show the disordered portion of the FG Nups. Techniques such as NMR and atomic force microscopy (AFM) can help gain insight into their conformational ensembles, as can some superresolution microscopy techniques, though the time and length scales of transport are often prohibitive for any microscopy [11–13]. Early research suggested that the FG Nups formed a central plug or “transporter,” but more recent work suggests that there is no central structure and the central channel is filled instead with highly dynamic disordered proteins [12, 14, 15]. There is some evidence from simulations that the density of the FG Nups, as well as their charge density and hydrophobic properties, are not uniform along either the radial or axial directions [16–18]. This may contribute to selective transport, although the pore still functions without the asymmetric FG Nups [19]. Indeed, the NPC is remarkably robust to FG Nup deletion. Over half of the mass of FG Nups can be removed without eliminating the selectivity barrier [19–22].

Transport factors are ordered proteins that carry cargo through the NPC. While there are various types, they share several features in common, most notably the fact that all known transport factors have more than one hydrophobic binding pocket which binds to FG repeats. Binding affinities between transport factors and FG Nups are surprisingly difficult to measure accurately. Values of the dissociation constant K_D measured outside of the cellular context are often in the low nanomolar range, implying a binding lifetime which is inconsistent with the experimentally-observed rapid translocation through the nuclear pore [23, 24]. Recent consensus is that binding is much weaker in the cellular environment, with K_D values between hundreds of micromolar and millimolar, and with some transport factors additionally being actively released from the

pore [25–27]. The extreme binding multivalency of Nup - transport factor interactions adds a further layer of complexity to interpreting affinity data. It is increasingly accepted that the highly transient and multivalent binding of transport factors to FG Nups is key to the combination of high specificity and rapid transport exhibited by the NPC [28].

The karyopherins (Kaps), also known as importins and exportins, are largest family of transport factors. The approximately twenty different Kaps are responsible for most nucleocytoplasmic transport [29]. Kaps typically consist of multiple HEAT repeats, a helical motif which conveys structural flexibility [30]. Most Kaps bind their cargo directly via a nuclear localization signal (NLS, for nuclear import) or nuclear export signal (NES, for nuclear export). NLS and NES are relatively short amino acid tags found on cargo [31]. However, sometimes the adaptor protein importin α is also needed. In general, Kaps are on the order of 100 kDa in size, well above the passive permeability limit [1]. As discussed below, there is evidence that the presence of Kaps contributes to the selectivity barrier [29, 32–34]. Many Kaps must be actively released from the nuclear pore and from their cargo after transit [35, 36].

Unlike the karyopherins, nuclear transport factor 2 (NTF2) does not transport a wide variety of cargo across the NPC. Instead, NTF2 maintains the Ran gradient needed for transport by carrying the protein RanGDP across the pore [37, 38]. NTF2 is a homodimer whose monomers are 14 kDa and contain at least one FG binding site apiece. Although its small size of 28 kDa is near the 30 kDa cutoff for passive transit through the pore, its flux through the pore is still at least 30 times that of similarly-sized proteins that do not bind to FG Nups [39–41]. NTF2 does not require adapter proteins or active release from the pore. We predominantly use NTF2 as a model transport factor in both the theoretical and experimental work discussed here, because of its simplicity as well as its ease of expression and purification from bacterial cells.

Selective transport requires an energy source, which in the case of the NPC is provided by the Ran cycle. When a transport factor-cargo complex passes from the cytoplasm into the nucleus, it encounters a Ran carrying GTP (RanGTP) on the nuclear side which binds to the transport factor and displaces the cargo, actively releasing it. Then the transport factor-RanGTP

complex can collect a cargo destined for nuclear export, and this ternary complex can diffuse back through the NPC to the cytoplasm. The protein RanGAP then hydrolyzes the RanGTP to RanGDP, disrupting the complex into its three original pieces. Ultimately, the energy source for selective nuclear transport comes from the RanGTP-RanGDP gradient between the nucleus and the cytoplasm. This gradient is maintained partially by NTF2, which carries RanGDP through the pore. In the nucleus, RanGDP is returned to its RanGTP state by RanGEF, a protein which is localized to the nucleus [28, 37, 42]. Therefore, even though there is no directionality to NTF2-RanGDP transport, the effect is to replenish the pool of RanGTP in the nucleus. From the perspective of transport, this means that, for many molecules, the process of passing through the pore is itself passive and does not consume energy. The selectivity ultimately arises from concentration gradients maintained by the Ran cycle, but the selective mechanism does not itself actively require energy input.

One surprising feature of nuclear transport is its sheer speed and volume. The high macromolecular traffic between nucleus and cytoplasm requires high flux through each NPC. Experiments with permeabilized cells estimate that the total molecular flow through the NPC could be as high as 10-20 MDa per pore per second, corresponding to 100-1000 transport events per pore per second [39]. Experiments focusing particularly on NTF2 report fluxes between 50 and 250 molecules per pore per second [39–41]. Fluxes this high mean a continuously high occupancy of the NPC, estimated at up to 100 karyopherins at once [43]. One reason that individual NPCs can accommodate such high flux is the rapidity with which molecules transit the pore. A wide range of transport factors and cargo have a dwell time of less than 10 ms in the pore [13, 44–46].

1.1.3 Models of nuclear transport

While the components of nuclear transport are well-understood, questions remain regarding the mechanism behind its unusual selective properties. Broadly speaking, two of the most important theoretical frameworks are the hydrogel model and the entropic barrier model (Fig. 1.2). Both are supported by some experimental results and challenged by others, and they are not mutually

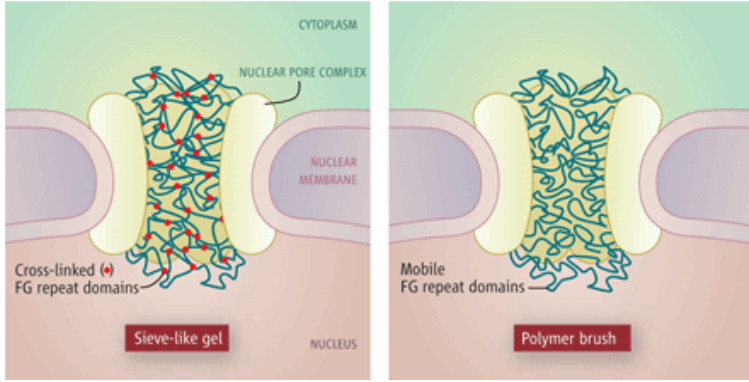


Figure 1.2: The two major models of the nuclear pore: the hydrogel (sieve-like gel) and entropic barrier (polymer brush) models. Figure from [47].

exclusive. More recent work suggests that the environment of the nuclear pore is somewhere between these two extremes.

The hydrogel model posits that the FG Nups within the nuclear pore are transiently crosslinked at their FG repeats into a hydrogel-like structure. Inert proteins are prevented from passing through the pore due to the small mesh size, while transport factors carrying cargo can bind to the FG repeats, disrupting the hydrogel and moving through the pore. This view of the nuclear pore is supported by experiments showing that the disordered domain of the essential FG Nup Nsp1 aggregates into a hydrogel when purified into buffer [48]. These hydrogels show strong selectivity for import of transport factors and their cargo over inert proteins, demonstrating binding between the aggregated FG Nups and the transport factors [49–51]. Theoretical models of diffusion through a transiently-crosslinked hydrogel show selective properties [39, 52, 53]. However, while nuclear pore mimics which consist of aggregated FG Nups display highly selective entry of transport factors, they do not permit the exit of transport factors over timescales consistent with transport [49, 50]. Furthermore, some Nups which aggregate in buffer remain disordered in the cellular environment [11].

Conversely, the entropic barrier model supposes that FG Nups instead act as polymer brushes within the pore. In this view, inert proteins are prevented from entering the pore due to the entropic penalty they would incur by restricting the possible conformations of the Nups. However, the decrease in free energy upon a transport factor binding to a Nup offsets the entropic penalty and allows transport factors and their cargo to pass [54, 55]. Evidence for this view comes from a number of studies in which single layers of FG Nups are grafted onto a surface and their extension

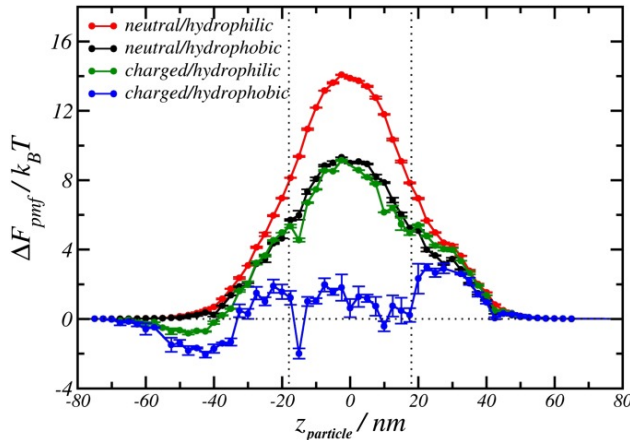


Figure 1.3: Example of effective-potential model of nuclear transport. Figure shows simulated free-energy landscape for a variety of possible transport factors as a function of position within the nuclear pore. Figure from [18].

monitored as transport factors are titrated on and off the surface [56–58]. Layer height tends to change non-monotonically as transport factors are added, suggesting that the presence of transport factors affects the selectivity of the nuclear pore.

More generally, FG Nups exist on a continuum of “cohesiveness,” ranging from Nups (or portions of Nups) which do not aggregate under any physiological conditions to ones which do so readily [11]. Nup cohesiveness depends on their charge, length, and hydrophobicity. Many simulations of the nuclear pore aim to understand the role of Nup cohesiveness in transport [18, 53, 59, 60]. A relatively common method of modeling transport is to computationally reduce the problem to that of a transport factor diffusing in a one-dimensional effective potential representing its interactions with Nups (Fig 1.3) [1, 18, 61, 62]. These models predict selective transport while being highly dependent on the precise details of Nup composition and location within the nuclear pore. These models also do not presuppose that either the hydrogel or entropic brush model is fully correct, but allow for a mixture of cohesive and non-cohesive Nups.

Apart from the question of FG Nup conformation within the nuclear pore, the role of transport factors themselves in the permeability barrier has been under investigation [29, 32–34]. There is evidence that the presence of karyopherins in the nuclear pore increases its selectivity for transport factors, possibly by establishing “tight-binding” and “weak-binding” subpopulations of Kaps which compete for binding sites on the Nups [56]. Even nonspecific competition may make the nuclear pore’s selectivity barrier more robust as well [63–66]. The precise role of crowding and competition

in nuclear pore selectivity is fascinating but as yet unclear.

Relatively few non-computational, quantitative theories of nuclear transport exist. Reaction-diffusion models have been proposed with varying degrees of complexity and different underlying assumptions but they do not take both binding kinetics and binding site saturation into account [61, 67].

1.1.4 Nuclear pore mimics

Many strategies have been used in attempts to create nuclear pore mimics which reproduce the selectivity properties of the nuclear pore. These generally fall into two categories: solid-state nanopores grafted with FG Nups, and hydrogels either made entirely of or filled with FG Nups. The hydrogel systems in particular are successful at showing selective entry of transport factors as compared to inert proteins but cannot be used to directly measure the material's selectivity.

Some synthetic nuclear pores recreate the nanopore geometry of the NPC using a perforated membrane which is coated in FG Nups. One such solid-state nuclear pore mimic consisted of the FG domains of Nsp1, Nup98, or Nup153 grafted onto a porous silicon nitride membrane [21, 68]. Transit events of transport factors or inert proteins through the bare or coated pores can be measured by monitoring the conductance of the pore, which spikes when a protein passes through. The flux of inert proteins drops significantly when the pore is coated with Nups, but that of transport factors remains roughly constant, suggesting selective transport [68]. Another nanopore NPC mimic used pores of varying diameter in 15-nm-thick polycarbonate membranes [22]. A portion of the pore was coated in gold to which FG domains of Nsp1 or Nup100 were conjugated. Measurements of flux through these pores showed a maximum of \sim 3-fold selectivity for NTF2-GST as compared to the similarly-sized inert protein BSA. Similar selectivities were seen for Kap95 with and without cargo. The FG Nup concentration could be tuned by varying the extent of the gold coating; increasing the Nup concentration increased the selectivity. Solid-state nanopores are the only nuclear pore mimic where selectivity has been directly shown; these selectivities are fairly low relative to that shown by the nuclear pore itself.

One class of hydrogel nuclear pore mimics consists of aggregated FG Nup domains. The FG repeat domain of Nsp1 will spontaneously aggregate into a hydrogel in buffer at physiological pH, as will the GLFG domains of Nup49p and Nup57p [48,69]. When these hydrogels are challenged with fluorescent transport factors or transport factor - cargo complexes, they show strongly selective influx as compared to inert proteins, with in-gel concentrations reaching 1000 times that of the reservoir surrounding the gel [49]. These hydrogels have amyloid-like characteristics and immobilize the FG Nups to a large degree, as shown by fluorescence recovery after photobleaching (FRAP) studies [48,50]. In addition to transport factors partitioning into the gel, other FG Nup domains become incorporated into the gel when introduced to the surrounding reservoir [48]. Gelation and selective influx are both destroyed by mutating the phenylalanines of the FG motifs to serines, indicating that interactions between FG repeats are necessary for these features [49]. While the selective influx is quite dramatic, direct measurements of diffusion constant or flux through an FG Nup hydrogel have not been made. Appendix ?? shows the estimated selectivity of several FG Nup hydrogels as predicted by our model described in Chapter ???. Some gels reach predicted selectivities of ~ 200 , within the range observed in the nuclear pore [39–41].

Other nuclear pore mimics also make use of hydrogels, but incorporate FG Nups as only one component of the gel rather than its entirety. Once such hydrogel was composed of a portion of the FG domain of Nsp1 fused to a domain that forms pentamers [51]. A fluorescent cargo targeted by Kap95 showed strong selective influx into these hydrogels, though equilibration was not achieved over the timescale of the experiments. The length of the FG Nup fragment used was varied so as to contain one, two, or six FSFG motifs, and the extent of binding of the transport factor-cargo complex to the gel was shown to depend on the number of binding motifs used. Predicted selectivities of these hydrogels are also shown in Appendix ??.

Other hydrogel nuclear pore mimics used an inert hydrogel as a scaffold to which fragments of FG Nups or other disordered peptides were tethered. Selective influx of the transport factor fusion protein GFP-Kap95 was shown for an acrylamide hydrogel containing high concentrations (250-400 mM) of stand-alone FSFG motifs, not incorporated into a longer peptide [70]. Increasing

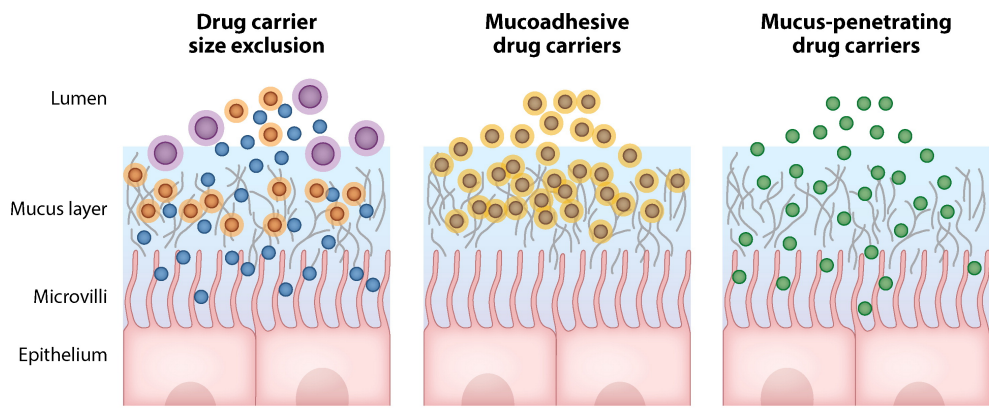
the concentration of FSFG anchored to the hydrogel increased the partitioning of GFP-Kap95 into the gel, but the influx was relatively low given the high concentration of FSFG motifs in the hydrogel. Other hydrogel mimics used engineered peptides with similar properties as those of FG Nups but not derived from them [67]. These were tethered to a PEG hydrogel and bound a fluorescent antibody (approximately 150 kDa) with varying affinity. The influx of antibody into the hydrogels showed a non-monotonic dependence on affinity, with an optimal dissociation constant $K_D \approx 30 \mu\text{M}$. FRAP measurements confirmed that binding antibodies diffused more slowly in the gel than did inert control proteins.

An interesting preliminary work demonstrated the use of DNA origami to mimic the scaffold of the nuclear pore by assembling DNA into a ring 46 nm in diameter and 14 nm in height, with up to 48 sites for FG Nup attachment [71]. When FG domains of Nsp1 or Nup100 were anchored to the attachment points, AFM confirmed that the Nups filled the center of the ring and remained highly dynamic.

While nuclear pore mimics, especially hydrogel-based mimics, show strong selective influx of transport factors, direct measurements of selectivity have remained largely unavailable.

1.2 Other selective biofilters

Selective biofilters exist in many contexts outside of nuclear transport, and they frequently include a common set of elements that are exemplified by the nuclear pore. In particular, cells often need proteins to move rapidly within a cellular compartment but still possess high binding specificity. This is often accomplished with intrinsically disordered proteins that interact transiently and multivalently with their binding partners. In the crowded environment of the cell or extracellular matrix, nonspecific binding can immobilize proteins, hindering selective motion, unless those proteins are able to continue diffusing while bound, a feature which we argue is key to the selective transport of the NPC as well as the biofilters discussed here. The following section presents three particular examples of selectivity in biological systems, from widely disparate areas, which bear striking similarities to the selectivity of the nuclear pore. In the remainder of this work, we model



 Carlson TL, et al. 2018.
Annu. Rev. Biomed. Eng. 20:197–220

Figure 1.4: Nanoparticle drug delivery through a mucus barrier. Particles which are too large cannot pass the size-exclusion barrier. Mucoadhesive particles penetrate the mucus layer but are trapped by binding interactions. Inert mucus-penetrating particles have a much higher diffusion constant in mucus. Figure adapted from [72, 73].

selective transport using a minimal set of characteristics that, while inspired by the nuclear pore, apply to the systems described here as well.

1.2.1 Drug delivery through mucus barriers

One medically-important selective biological barrier is the mucus which lines organs such as the lungs, nose, and stomach. In particular, lung mucus presents a barrier to delivery of inhaled medication. If nanoparticles containing drugs for lung diseases such as asthma and lung cancer could be inhaled and taken up by lung cells, doses could be lower, as the uptake would be more targeted [72, 74]. However, lungs are coated by a layer of mucus intended to prevent foreign objects from reaching the lung cells. In order to deliver nanoparticles to lung cells, they must be engineered to pass the selective mucus barrier.

Mucus consists predominantly of disordered glycoproteins known as mucins, though other components such as lipids are present as well [75]. These entangled mucins present multiple barriers to nanoparticles, as shown in Fig. 1.4. First, large particles are excluded due to the 150-350 nm average pore size of mucus gels [76, 77]. Second, even particles which are small enough to enter the mucus layer often bind to mucins. In fact, mucoadhesive particles (MAPs) have been specifically

engineered on the principle that increasing the nanoparticle's lifetime within the mucus will lead to more efficient drug delivery [78]. However, diffusion of MAPs is often so slow that they do not penetrate beyond the edge of the mucus layer. Furthermore, mucus gradually replaces itself on clearing timescales which vary depending on the type of mucus. Nanoparticles in the outermost region may be cleared more rapidly than those which diffuse deeply into the mucus layer, however, the rate at which mucus clearance depends on depth within the layer is uncertain [79–81].

Another approach for nanoparticle delivery through the lung mucus barrier makes use of small, inert particles which minimize nonspecific interactions with mucins. These mucus-penetrating particles (MPPs) are typically coated in PEG or another inert polymer [74, 82]. MPPs can reach much higher diffusion constants in mucus than can MAPs [77, 83–85]. For instance, 500-200 nm particles coated in PEG had a diffusion constant in mucus thousands of times higher than similarly-sized uncoated particles [77]. PEG-coated nanoparticles under 300 nm are retained in mouse lungs 2-3 times longer than uncoated particles [74].

The selective barrier of lung mucus bears similarities to the selectivity of the nuclear pore in that it consists of disordered proteins which bind to particles impinging on the barrier. However, in the case of mucus, binding inhibits the flux of particles through the selective filter, while binding enhances the flux of transport factors through the nuclear pore. A better understanding of the role of binding and bound diffusion to a selective filter such as the nuclear pore could suggest novel strategies for nanoparticle delivery through lung mucus. Perhaps binding can be used in a way that enhances nanoparticle flux over that of inert particles, improving drug delivery to the lungs.

1.2.2 Diffusion of DNA-binding proteins in the nucleus

Principles of selectivity appear in biological systems beyond straightforward filtering. In particular, transient binding and bound-state diffusion are important to DNA targeting in the nucleus by transcription factors and DNA damage repair proteins. A protein diffusing in the cell's nucleus has many of the same constraints and capabilities as a transport factor passing through the nuclear pore: it is surrounded by a high concentration of flexible tethers to which it binds transiently.

Just as this situation leads, counterintuitively, to high flux of transport factors through the nuclear pore, DNA-targeting proteins find their specific targets much more rapidly than would be naively predicted [86]. For example, the zinc-finger transcription factor Egr-1 appears to locate its target DNA within a few minutes of arriving in the nucleus, despite observed micromolar affinities for nonspecific DNA sequences [87].

Solutions to this “needle in the haystack” challenge resemble possible mechanisms of bound diffusion in the nuclear pore complex. In particular, it is widely accepted that the search for targets is made more rapid through facilitated diffusion, involving proteins sliding along strands of DNA. However, the optimal time spent in a one-dimensional search as opposed to a free three-dimensional search is unclear; as is the effectiveness of sliding as opposed to multiple, rapid binding and unbinding events [88]. This mechanism is reminiscent of both the sliding mechanism predicted in some transport factors and of the effect of diffusion while bound to a flexible tether [89]. Additionally, transfer of a multivalent transcription factor between two strands of chromatin, a mechanism known as intersegmental hopping, can increase the protein’s search space similarly to the multivalent inter-Nup hopping that is available to transport factors [90, 91]. Finally, transient binding plays an important role in the search for DNA targets. This speed-stability paradox reflects the fact that, like in the nuclear pore, proteins must bind very weakly to their DNA tethers to avoid becoming immobile. Unlike nuclear transport, however, DNA-binding proteins must bind more tightly to their targets upon reaching them [87, 92].

A case in point, further discussed in Sec. ??, is that of poly(ADP-ribose) polymerase 1 (PARP1), a DNA damage repair protein which rapidly localizes to sites of DNA damage. PARP1 binds damaged DNA with low nanomolar affinities, and appears to bind undamaged DNA only a few orders of magnitude more weakly [93]. Given that there are up to 5 mM nonspecific DNA binding sites in the nucleus, the speed with which PARP1 diffuses (~ 10 times slower than in buffer) is remarkable [87]. PARP1 contains multiple DNA-binding sites, and an inter-strand hopping mechanism has recently been demonstrated, which may explain its rapid diffusion [94]. However, removal of that mechanism only slightly slows the recruitment of PARP1 to sites of DNA damage,

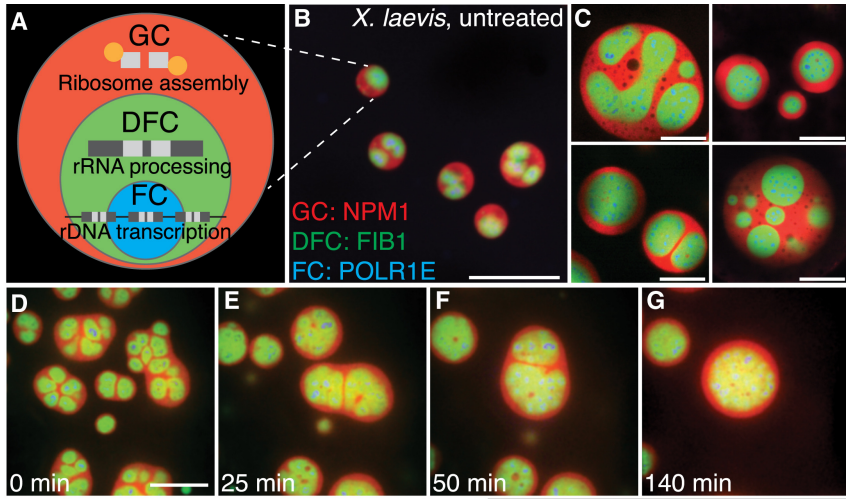


Figure 1.5: Phase-separated subcompartments of *Xenopus* nucleolus. (A) Schematic of subcompartments. (B)-(C) Fluorescence microscopy image of nucleoli with subcompartments in red, green, and blue. (D)-(G) Time-course showing dissolution of compartments after actin disruption. Figure adapted from [96].

suggesting that a further mechanism of bound-state diffusion is necessary [95]. The principles of selective nuclear transport may help to explain the rapid motion of PARP1, along with other DNA damage repair proteins and transcription factors.

1.2.3 Subcompartments in liquid droplets

Features of nuclear transport such as highly-concentrated disordered proteins and bound-state diffusion also appear in liquid-liquid phase separated droplets. Liquid-liquid phase separation as a driving force for the formation of membraneless organelles is rapidly gaining prominence. It is becoming clearer that many cellular functions are regulated through the phase separation of mixtures into phase rich in various proteins and other cellular components. Membraneless organelles include nucleoli, which aid in processing ribosomal DNA genes within the nucleus, and RNA granules, which help sort mRNA [6, 97].

Liquid-liquid phase separation typically occurs for mixtures containing IDPs with multivalent interactions, described as “sticker” and “spacer” regions, similar to the hydrophobic FG repeats and hydrophilic linker regions in FG Nups [98]. For example, the disordered protein FUS, widely studied for its phase separation behavior, consists of interacting regions rich in tyrosine and arginine separated by linkers enriched in glycine and serine [99]. Dense liquid phases are highly concentrated, but the proteins that comprise them remain mobile. There are subcompartments of varying

composition within some membraneless organelles, which may be due to liquid-liquid phase separation. Nucleoli contain multiple subcompartments which are thought to perform distinct functions (Fig. 1.5) [96, 100, 101], while RNA granules have recently also been shown to have a core-shell structure [97, 102].

Much of the current work on liquid-liquid phase separation in subcompartments of membraneless organelles is going towards simply identifying the components of the compartments [101]. Discussion of their purpose and mechanisms is still quite speculative. However, it seems plausible that one function of these compartments is to selectively concentrate enzymes or other proteins to increase reaction rates. RNA bodies in particular are known to sort and sequester mRNA [97]. As such, the presence of disordered, multivalent proteins may not simply be necessary for the formation of phase separated droplets, but could potentially assist in selectively filtering the components of the subcompartments. If nuclear transport is a guide, binding partners of the IDPs which form the outermost phase might have a higher flux into the inner compartments than nonbinding proteins. Additionally, in the context of bound-state diffusion, liquid droplets represent maximal bound diffusion, as binding to an IDP in solution will not appreciably slow the diffusion of the binding partner. While these possibilities will not be testable for some time, membraneless organelles may prove to be a fascinating application of selective biofiltering.

1.3 Project goals and motivation

All of the systems described above involve the rapid flux of proteins which still bind highly selectively to their environment. We wondered whether there were simple features, such as such as transient, multivalent binding to flexible, dynamic tethers, could explain this apparent paradox. We approached the problem through both modeling and experiment and identified a common key parameter in the form of bound-state diffusion. While the theory and experimental setup were based on nuclear transport, both platforms are general enough to apply to a number of selective biofilters.

1.3.1 Minimal model of selective transport

Despite the complexity of nuclear transport, many components can be removed or approximated without eliminating its unusual selective properties. For example, Nups which are asymmetrically distributed along the axis of the nuclear pore can be removed, as can a large fraction of Nups overall, without destroying selectivity [19–22]. And though many transport factors require active release from the pore, others, such as NTF2, do not; selectivity is not therefore dependent on active release. We decided to model the pore in order to answer the question: What are the minimum requirements for selective transport?

In the course of creating the model, we found that one possible set of minimum requirements are quite simple indeed. The model discussed in Chapter ?? not only dispenses with non-uniformly distributed Nups and facilitated release, but also with nonspecific crowding, Kap-centric control of the nuclear pore, the Ran cycle, and even the nanopore geometry. Instead, the pore is treated as a bulk material of finite thickness with an artificially-imposed concentration gradient to drive flux across it. Competition for binding sites is retained in the form of binding site saturation, but even without this feature we see selective flux across the barrier. Our model fundamentally contains only diffusion and binding of transport factors to Nups - an extremely streamlined depiction of nuclear transport, and one that can even be treated semi-analytically.

The simplicity of our model made the key parameter clear: we could not reproduce the selectivity of the nuclear pore without allowing bound-state diffusion, that is, assuming that bound Nup - transport factor complexes were mobile within the pore. Bound diffusion provides a possible answer to the paradox of nuclear transport, resulting in a higher flux of transport factors, which bind to Nups, than inert proteins which do not. In our model, this straightforward mechanism alone gave rise to the decidedly unintuitive behavior of the nuclear pore.

Having identified bound-state diffusion as an important parameter for selective filters, we investigated possible methods of bound diffusion within the nuclear pore. Two possibilities arose from basic, well-accepted facts of nuclear transport: tethered diffusion arising from the disordered,

flexible nature of the Nups, and inter-chain hopping of the transport factor due to its binding multivalency. Upon investigation, both mechanisms can plausibly provide the high bound diffusion constant needed to reproduce the selectivity of the nuclear pore.

While this model was inspired by nuclear transport, it ultimately relies on only a few key properties of the system. With this model, we predict selective transport will occur where there is bound-state diffusion, which can be readily obtained if flexible IDPs are present for tethered diffusion, or if highly transient, multivalent binding allows for motion from one site to another while remaining bound. The systems described above in Sec. 1.2 fall into this category, as likely do many others. Furthermore, these principles might guide synthetic selective biofilters with novel rapid, highly-selective properties.

1.3.2 Experimental tests of bound-state diffusion in biomaterials

After developing the minimal model of selectivity, we began developing a synthetic biofilter with which to experimentally probe the effect of bound-state diffusion on selectivity. The model itself is sufficiently general to apply to a wide range of filters, giving us some freedom in designing a material to test its predictions. We chose to use the nuclear pore as inspiration for this material because its key components are so well known, if not well understood. In order to capture the key features of selectivity, we designed hydrogels containing peptide tethers derived from FG Nups. The transport factor NTF2 served as a test protein whose diffusion we could compare with a similarly-size but nonbinding counterpart. These hydrogel nuclear pore mimics display the mechanisms that lead to selective transport in our model: flexible, dynamic tethers which can transiently bind to transport factors, along with multivalent transport factors which can “hop” between peptide chains without fully unbinding. We predicted that these features will be sufficient for bound-state diffusion of the transport factor within the hydrogel.

As with the theoretical model, many of the NPC-specific details, such as the nanopore structure and Ran gradient, were omitted. A bulk material was used instead of nanopores because our model should apply equally well to both, and a macroscopic hydrogel is much easier to study.

We quickly realized that hydrogels are a challenging system to use for protein separation. The nuclear pore mimics have a rigorous set of competing constraints: for example, the hydrogel should be in mechanical equilibrium and homogeneous, while still well-sealed to a flow chamber so that proteins cannot bypass the gel. Chapter ?? documents the design of the hydrogel nuclear pore mimics. Many modifications intended to improve the diffusion properties and reproducibility of the hydrogels proved unsuitable for our needs. However, we eventually produced a biomaterial that can be used to measure bound diffusion, while also developing more general guidelines for designing hydrogels that are useful for protein separation.

The resulting bound-state diffusion measurements are presented in Chapter ???. Fluorescence recovery after photobleaching (FRAP) was used to determine the effective diffusion constants of both NTF2 and an inert protein, from which the bound diffusion constant was calculated. The data analysis ultimately required a two-dimensional Fourier series solution to the diffusion equation, resulting in a set of data-processing scripts which can be applied to any circular material undergoing equilibration with a fluorophore. We measured a non-zero bound diffusion constant that is consistent with the predictions of our model and tested the effect of varying Nup length on bound-state diffusion. Our results indicate that these nuclear-pore-inspired hydrogels can be used to probe the effect of our model's parameters on bound diffusion.

While bound diffusion is a key parameter in our selectivity model, the aggregation state of the Nups could also affect selectivity. Aggregated Nups will be less dynamic and effectively act as shorter tethers, limiting bound diffusion. In Chapter 2, we probed the aggregation behavior of an FG-Nup-derived peptide in several crowded conditions. Using a fluorescent amyloid assay, we identified significant differences in the aggregation dynamics in the presence of different crowding agents, including between poly(ethylene glycol) (PEG) and polyvinylpyrrolidone (PVP), two inert polymers that are widely presumed to be interchangeable as crowders. We followed this aggregation assay with NMR and fluorimetry studies in order to investigate the nature of the changes. The results suggest that the presence of an aromatic ring in PVP may interact with the phenylalanines in the FG motifs of the peptide, changing its local chemical environment and therefore its aggregation

behavior.

Although a true hydrogel-based selective biofilter proved challenging to design, our nuclear-pore-inspired material can be used to measure the bound-state diffusion of proteins. This parameter is likely important to a variety of problems involving rapid transit of highly-selective proteins. Hopefully the model and biomaterials developed here can be used to investigate these systems more generally in the future. This work suggests that bound-state diffusion, particularly when resulting from transient, multivalent binding, may explain a number of unusual biological filters.

1.4 Biophysics is beautiful

Even beyond the ample practical reasons to study nuclear transport, it is a fascinating process, full of counterintuitive results and apparent paradoxes. The nuclear pore is at once an incredibly intricate nano-machine and surprisingly robust to perturbation. Passage through the nuclear pore is carefully controlled by complex cellular processes, yet the mechanism of selectivity itself does not require energy input. Nuclear transport can enhance the flux of transport factors hundreds of times over that of inert proteins using a mechanism that conventionally *reduces* protein mobility.

Where the NPC is not apparently self-contradictory, it is a picture of extremes. FG Nups are not only disordered, many show virtually no signs of secondary structure whatsoever and do not order appreciably upon binding transport factors. Nup - transport factor binding is extreme on many axes: the affinity, likely in the millimolar range, is weak enough that most biochemists would characterize it as nonspecific binding, yet it permits a high flux through the pore. At the same time, the on-rate is ultrafast, bounded by the physical diffusion limit rather than chemical considerations. Finally, with dozens of FG motifs along the length of each Nup, and multiple binding pockets on each transport factor, Nup - transport factor binding is dizzyingly multivalent. It is perhaps no wonder that measurements of the binding affinity have historically spanned six orders of magnitude; at this level of multivalency, even the notion of “binding affinity” itself becomes difficult to define. In almost every respect, the binding interactions which underpin selective transport are as far removed as possible from textbook protein-protein interactions. The nuclear pore is a fundamentally *weird*

system and deserves to be studied purely for the joy of discovering how something so unusual operates.

Furthermore, the details of nuclear transport are all but invisible even to the most cutting-edge biochemical techniques. The timescale of transport is too fast, the size too small, and the disordered Nups too dynamic to permit direct visualization of transport. This is a system which practically demands to be studied using nontraditional, interdisciplinary methods.

There is value in approaching the nuclear pore specifically from the perspective of physics. Biophysics as a field experiences constant tension between the need to account for the incredible complexity of any living system and the drive to reduce it to its smallest, tidiest set of component parts. As a physicist, I take deep satisfaction from applying a broad and simple theory to a complicated system and still getting meaningful results. All of the messy intractable details are of course ultimately necessary for life to exist, but if a big, sweeping, absurdly simple, underlying principle can explain even 50% of a complex system, that's beautiful. Such opportunities abound in biophysics, from fruit flies which right themselves after mid-flight perturbation, to the scaling of barbs in cat tongues, to how cucumber tendrils coil and overwind, to the nuclear pore complex and more [103–105]. Sometimes it's worthwhile to apply basic physical theories to ridiculously complicated things which they manifestly cannot fully explain - valuable practical advances frequently arise from surprisingly slender foundations.

Whether viewed through a practical, intellectual, or aesthetic lens, there is much to be gained from the study of nuclear transport and, more broadly, of binding and diffusion in selective biofilters. Certainly I have found that, despite the setbacks and disappointments which accompany all research, I have never been able to describe my work to others without becoming truly enthusiastic yet again.

Chapter 2

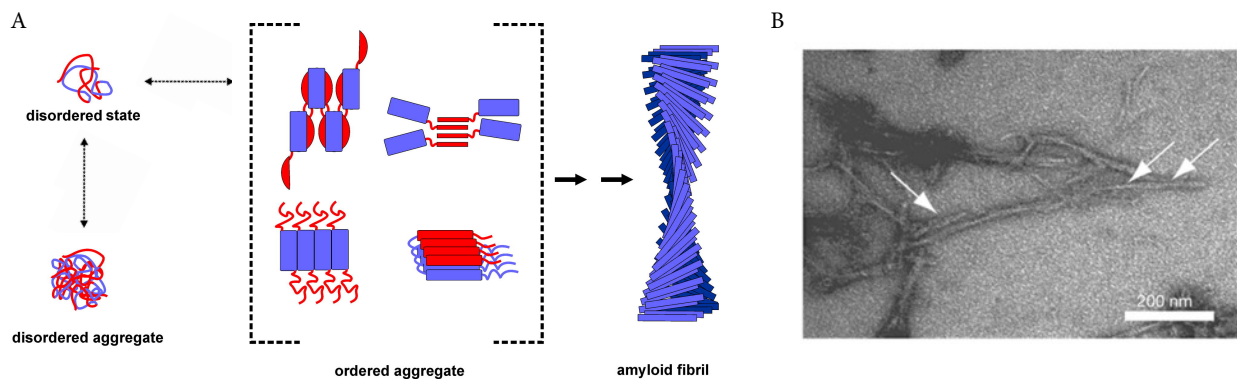
FG Nup aggregation under crowded conditions

While our bound-state diffusion model of selectivity is general enough to apply to many biofilters, we have been using the nuclear pore in particular as inspiration. We predict that its selective properties arise from the continued mobility of transport factors while bound to FG Nups. One mechanism of bound-state diffusion arises from the flexible, tether-like nature of the disordered Nups. Such a mechanism is possible whether the Nups form a polymer brush or a transient hydrogel, so long as they remain sufficiently dynamic.

The exact conformation of Nups within the nuclear pore is unknown, due to the difficulty in imaging such a disordered system. Some Nups, such as Nsp1, aggregate in buffer to form hydrogel structures [48–50], although evidence suggests it does not aggregate in the cellular environment [11]. Other Nups can form phase-separated liquid droplets [106]. Nup153 forms amyloid fibrils *in vitro* (Fig. 2.1B) at a rate which is increased by the addition of inert crowders [107]. Amyloid structures, as shown in Fig. 2.1A, are long chains of stacked β sheets which are much less flexible and dynamic than individual disordered proteins, potentially limiting the effectiveness of the tethered bound diffusion of transport factors. Amyloid fibrils are commonly formed by disordered proteins upon aggregation and are often implicated in disease [108]. On the other hand, atomic force microscopy (AFM) data and simulations suggest that Nups in the nuclear pore remain highly dynamic [12, 14].

We decided to test the aggregation behavior of a fragment of the essential FG Nup Nsp1 known as FG124, described in Sec. ?? and Appendix ???. This 124-amino-acid peptide contains

Figure 2.1: Aggregation of FG Nups into amyloid fibrils. (A) Schematic of possible aggregation states of a disordered protein, including disordered aggregates, intermediate amyloid-like states, and fibrils composed of stacked beta-sheets. Rectangles denote secondary structure. Figure adapted from [108]. (B) Negative-staining electron micrograph of amyloid fibrils consisting of the human Nup153 FG domain. Arrows indicate characteristic twists of the fibrils. Figure adapted from [107].



eight FG motifs and is known to aggregate in buffer over the course of several hours. However, in-cell NMR shows it to remain disordered inside bacterial cells [11]. Given the disparity in aggregation behavior under these different conditions, we wanted to determine whether we could encourage or suppress aggregation and amyloid formation with our choice of crowding agents.

While the simplicity of studying aggregation of FG124 in buffer alone is appealing, the nuclear pore is a very different environment. Cells are extremely crowded with proteins, nucleic acids, and other macromolecules. Some estimate that macromolecules fill 30% of a cell's volume [109]. Crowding can have strong effects on a protein's behavior, sometimes in surprising ways. Furthermore, crowding effects can differ depending on whether the crowders are inert, interacting, compact, extended, and so on. Generally speaking, crowding seems to increase the rate of aggregation of disordered proteins, but this is by no means universal [107, 109–112]. The presence of small crowders tends to encourage proteins to take on compact conformations due to the excluded volume effect, which in the case of IDPs often leads to aggregation. However, the viscosity changes due to crowding may inhibit the formation of aggregates [113, 114]. Crowding with proteins capable of nonspecific interactions has been shown to inhibit the partitioning of IDPs into phase-separated liquid droplets [115]. Other important but not well-understood factors include crowder structure and interactions, agitation or its absence, and the presence of an air-water interface [109, 111].

We studied FG124 aggregation in the presence of various crowding agents, both inert and nonspecifically interacting, using a number of techniques. The kinetics were probed with a fluorescence aggregation assay, which showed significant differences between crowders. Two inert crowders, poly(ethylene glycol) and polyvinylpyrrolidone, were chosen for further NMR and fluorescence spectroscopy. The results do not have a clear interpretation but suggest that the presence and type of crowding agent is indeed affecting the local chemical environment of the peptide's residues, including its phenylalanines. Given the importance of the FG repeats to Nup cohesiveness and transport factor binding, this could have implications for the optimal conditions under which to study Nup behavior *in vitro*.

2.1 Fluorescence time courses

In order to probe the aggregation kinetics of FG124, we incubated samples in the presence of crowders and thioflavin T (ThT), a dye which is sensitive to the presence of amyloids. Over the course of several hours, FG124 aggregated and the fluorescence intensity from ThT increased. By recording the intensity at 10-minute intervals, we were able to plot sigmoidal aggregation curves for the samples, as shown in Fig. 2.2. These curves show a lag phase while the aggregates are nucleating, followed by a growth phase of rapid aggregation, ending in a plateau phase. We recorded time-courses for multiple crowders, including inert crowders as well as nonspecifically binding ones, and analyzed the resulting aggregation parameters. Poly(ethylene glycol) (PEG) and polyvinylpyrrolidone (PVP) were chosen as representative inert crowders. Cell lysate was used to imitate the cellular environment and test the effect of nonspecific interactions on FG124 aggregation. Finally, serine was used as a crowder as previous work demonstrated that it caused Nup153 to aggregate more quickly [107]. Many of the timecourse experiments were performed by Sophie Reskin and Paul Marchando, and Sophie also took part in the analysis.

Thioflavin T is a dye that grows much brighter when bound to amyloids. Upon binding, its absorption maximum shifts from 385 nm to 450 nm and its emission maximum from 445 nm to 482 nm [116]. Although ThT is a more reliable indicator of amyloids than other fluorescence methods, notably Congo red stain, it suffers from reproducibility problems. There is no consensus on the mechanism of ThT binding to amyloids. Some proposed mechanisms rely on the presence of ThT micelles, which form above a critical concentration of about 4 μ M, while others advocate for avoiding micelles [117, 118]. There is some evidence that amyloid fibrils can adsorb to the plastic surface of a multiwell plate, decreasing ThT fluorescence intensity as the fibrils mature [119]. Often in our timecourse experiments, the ThT fluorescence did reach a maximum and then decrease. The fluorescence intensity also depends on the sample viscosity, an effect which we noticed in our timecourses [120]. Despite these challenges, thioflavin T is the most consistent dye for detecting the process of amyloid formation.

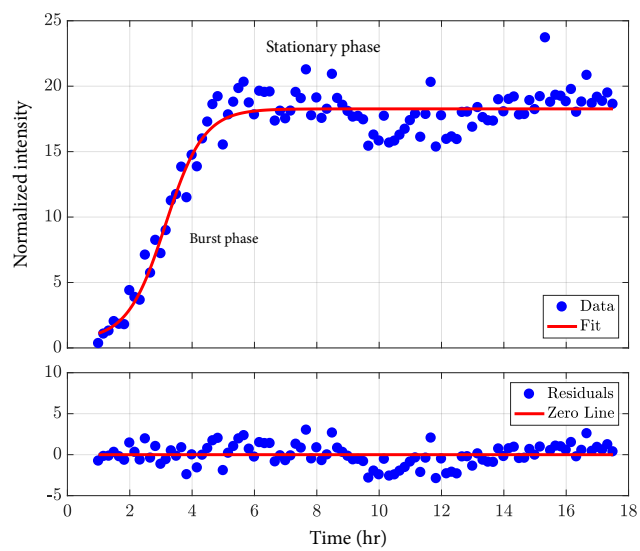


Figure 2.2: Sample sigmoid fit to FG124 aggregation timecourse with 13% w/v PEG. Burst phase and stationary phase are shown; lag phase took place before data collection began. Fit is to Eqn. 2.1.

2.1.1 Methods

2.1.1.1 Buffers

Potassium transport buffer (PTB) (150 mM KCl, 20 mM HEPES, 2 mM MgCl₂) was used for all timecourse and NMR samples.

2.1.1.2 FG124 preparation

His-tagged FG124 was expressed in *E. coli* in the plasmid pRSF. Cultures were grown in LB and induced at 37°C for 2-4 hr with 1 mM IPTG at OD 0.6-0.8. Periplasmic matrix was removed prior to lysis. Cells were then lysed via sonication and FG124 purified using TALON cobalt resin (Appendix ??). All purification buffers were PTB with 7M guanidine hydrochloride (GuHCl) and protease inhibitor cocktail (PIC). The elution buffer also contained 250 mM imidazole.

2.1.1.3 Timecourse preparation

Stocks of PEG (avg. MW 20 kDa, Sigma, Bio-Ultra) and PVP (avg. MW 40 kDa, Sigma) in PTB were prepared at 20 or 40% w/v; L-serine (EMD Millipore Calbiochem) stocks were prepared at 30% w/v. PEG and serine were at pH 7; PVP was pH 7 or pH 5. Lyophilized lysate was prepared by homogenizing BL21 DE3 Gold cells and spinning them down. The supernatant was lyophilized in a decomposing ammonium bicarbonate buffer and resuspended in PTB to the desired concentration when needed. A 10 mM stock solution of ThT in PTB was prepared and filtered no more than a week before the timecourse, stored at room temperature and protected from light. Immediately prior to starting the timecourse, FG124 was desalted into PTB to remove the imidazole and GuHCl. Samples were promptly prepared containing the appropriate percentage of crowder, a final concentration of 1-2 mg/mL FG124, and 200 uM thioflavin T. All samples in the same timecourse had the same concentration of FG124, including the buffer sample, which contained no crowding agent. Blanks were prepared with crowding agent and thioflavin T, but no FG124. Samples were pipetted into black, flat-bottomed, clear-bottomed 96-well plates with 150 uL per

replicate. Each sample yielded four to six replicates. Only one blank replicate was used per condition. One negative control and corresponding blank were prepared per timecourse containing 7M GuHCl and no crowding agent but using the same protein sample as all other conditions. Each well contained a 3mm-diameter glass or teflon bead. The plate was sealed with a PCR seal and taken to a Safire II plate reader. The fluorescence was measured from the bottom at 10-minute intervals with an excitation wavelength of 450 nm, emission wavelength of 482 nm, and 5 nm bandwidths. The plate shooook orbitally at high speed between measurements and was held at a temperature of 30 degrees C. The time between desalting and beginning the plate reader measurements was typically about an hour; the time of desalting was taken as $t = 0$ for the purposes of calculating lag time. In parallel with the sample preparation, the concentration of the desalted FG124 was measured with a BCA assay. Sophie Reskin helped to optimize this assay, making extensive use of [121].

2.1.1.4 Timecourse analysis

After carrying out the aggregation timecourse, the data were normalized and fit to a sigmoid function in order to extract aggregation lifetimes and lag times.

The data were first normalized to the blanks, which contained crowding agents but no protein. In nearly all cases, the blank intensity remained steady over time, as expected. In those cases, the mean blank intensity was subtracted from the corresponding data. In cases where the blank intensity changed over time, it was subtracted pointwise from the data.

Then the normalized curves were fit to a sigmoid given by

$$I(t) = C + \frac{A}{1 + \exp(-k(t - T_{1/2}))} \quad (2.1)$$

where $I(t)$ is the normalized fluorescence intensity as a function of time (Fig. 2.2). The aggregation dynamics are described by the rate k and the half-time $T_{1/2}$, which reflects the time needed for the intensity to reach half of its asymptotic value. More descriptive than the half-time is the lag time

T_ℓ , calculated as

$$T_l = T_{1/2} - \frac{2}{k} \quad (2.2)$$

and representing the duration of the lag phase [122]. The lag time here is defined as the intersection of the tangent line of maximum slope of the growth phase with the flat background signal of the lag phase.

The offset C and final amplitude A are less meaningful in this context, and less reliable. The offset should in principle be $C = 1$, as the fluorescence of the sample and its blank should be equal before aggregation has begun. Experimentally, $C \sim 1\text{-}2$, reaching a maximum near $C = 10$ for a few sample conditions. While this may have been because sample aggregation had already begun, the long lag times of those conditions do not support that interpretation. It is possible that the presence of the unaggregated protein caused a change in baseline fluorescent through an unknown mechanism.

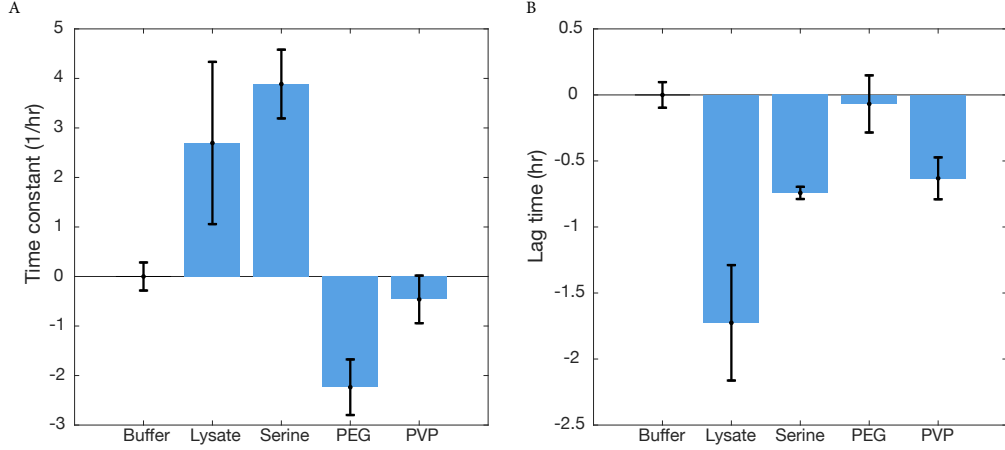
The plateau phase asymptotes to an intensity given by $I_\infty = C + A$. We found significant variation in I_∞ for the same condition between timecourses, and the relative magnitudes of different conditions also varied between timecourses. As seen in previous thioflavin T studies, higher viscosity tended to result in higher values of I_∞ . Therefore, we do not consider I_∞ in our analysis, leaving the aggregation rate k and lag time T_ℓ as parameters of interest.

Next we normalized once again to account for differences between timecourses. It was impossible to hold the FG124 concentration exactly fixed between timecourses. Final protein concentration varied between 0.3 and 2.5 mg/mL. Within each timecourse, we averaged the fit parameters for all replicates of FG124 in buffer only and subtracted that average from each replicate of each crowding condition.

2.1.2 Results

The mean fit parameters and number of replicates for each crowder condition are shown in Table 2.1 and Fig. 2.3. For both the aggregation rate k and lag time T_ℓ , a one-factor ANOVA rejected at the $p = 0.05$ level the null hypothesis that there was no difference between the means.

Figure 2.3: (A) Aggregation rates and (B) lag times for all crowding agents, normalized to the no-crowding condition. Crowder concentrations were 19% w/v serine, 13% PEG, 13% PVP, and approximately 10 mg/mL lysate. Lysate concentration varied somewhat between experiments. Error bars are standard error of the mean.



Two-tailed t-tests were then run comparing all conditions shown in Fig. 2.3. The resulting p -values were below 0.05 except for those comparing no crowder to PVP (rate), no crowder to PEG (lag time), and serine to PVP (lag time). All p -values are reported in Appendix ??.

Several timecourses were run without crowders at varying pH. Table 2.2 shows the resulting fit parameters, given as lifetime $\tau = 1/k$ and lag time T_ℓ . Six replicates were run of each pH condition. One-way ANOVAs fail to reject the null hypothesis at the $p = 0.05$ level, suggesting

Table 2.1: Mean aggregation rate and lag time for all crowding agents, normalized to no-crowder condition. Number of replicates is N . Errors are standard errors of the mean.

Condition	Rate k (1/hr)	Lag time T_ℓ (hr)	N
No crowder	0 ± 0.3	0 ± 0.1	32
Lysate	2.7 ± 1.6	-1.7 ± 0.4	16
Serine (19%)	3.7 ± 0.7	-0.7 ± 0.05	28
PEG (25%)	-1.9 ± 0.4	1.7 ± 1.3	7
PEG (20%)	-0.3 ± 0.3	0.8 ± 0.7	7
PEG (13%)	-2.2 ± 0.6	-0.07 ± 0.2	31
PEG (5%)	0.2 ± 1.0	-0.6 ± 0.3	7
PVP (25%)	0.2 ± 2.6	2.7 ± 1.2	7
PVP (20%)	-1.1 ± 0.5	0.9 ± 0.7	6
PVP (13%)	-0.5 ± 0.5	-0.6 ± 0.2	32
PVP (5%)	-0.9 ± 0.6	-0.5 ± 0.3	7

that FG124 aggregation is not affected by pH in the range 5-8.

Two crowders, PEG and PVP, warranted special attention. These inert crowders are commonly used interchangeably, but the results of timecourses containing 13% PEG or PVP suggest that they may in fact affect FG124 differently (Fig. 2.3). In order to investigate any differences between PEG and PVP, timecourses were run with varying crowder concentrations and analyzed as before. Mean parameter values are shown in Fig. 2.4. Statistics are given in Appendix ?? but do not strongly suggest differences between varying concentrations within the same crowder.

2.1.3 Discussion

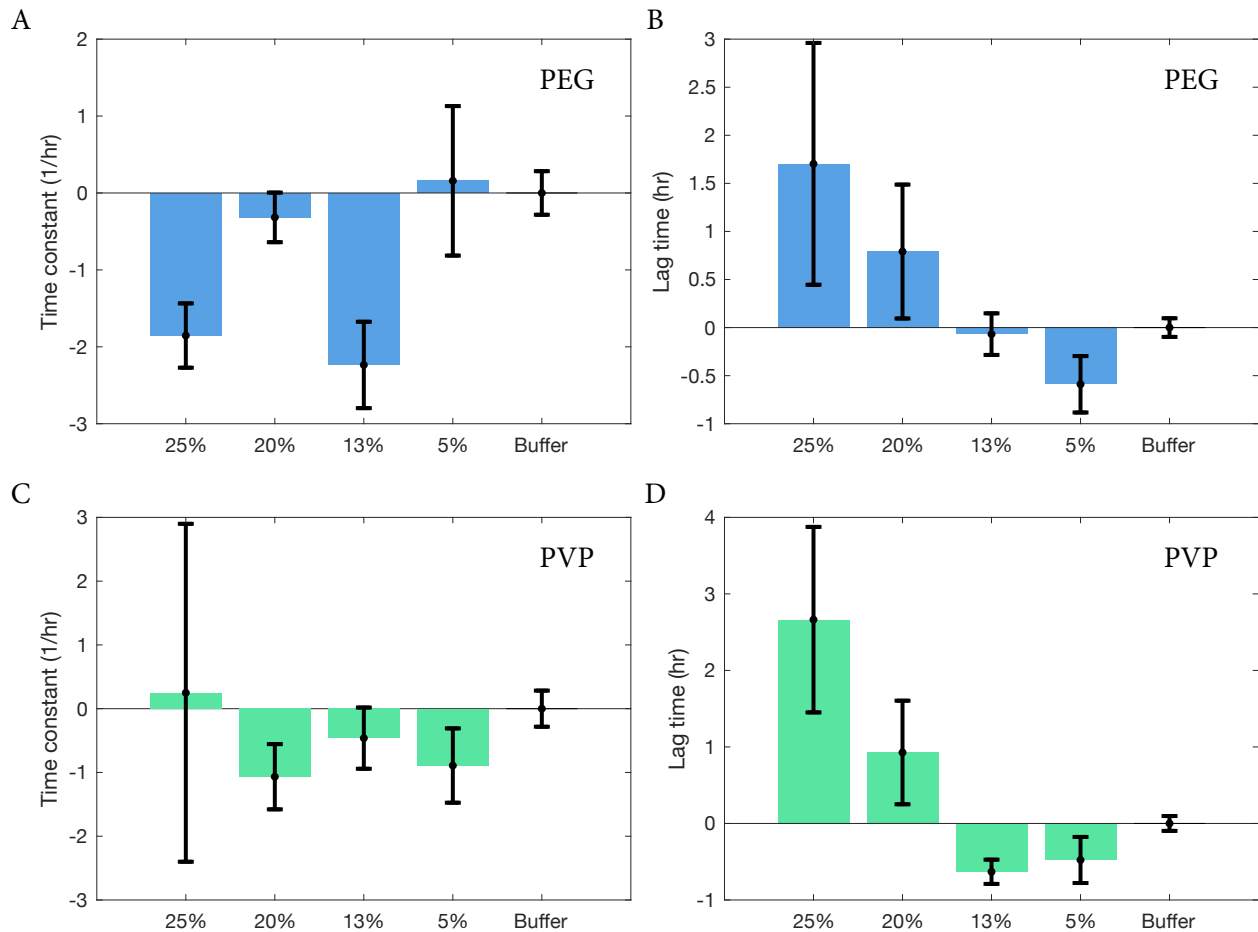
The results of the FG124 aggregation timecourses were difficult to interpret. The reproducibility of thioflavin T fluorescence assays is notoriously poor, and many timecourses were run with high variability in results. Results became more reproducible once the protocol was modified to include a bead in each well, which seemed to assist with mixing during the shaking incubation between time points. Only data taken after this change are included in this dataset.

The results indicate changes in both lag time and aggregation lifetime of FG124 as a result of changing crowder conditions. The origin and magnitude of these changes is unclear. We chose to target the crowders PEG and PVP for further investigation. These crowders, while typically treated as interchangeable, behaved differently in during the fluorescence timecourses (Fig. 2.3). When added to FG124 at a final concentration of 13% w/v, PEG reduced the aggregation rate below that of the no-crowder condition while PVP did not. Conversely, the lag time of the PEG condition remained approximately that of the no-crowder condition, but the lag time of the PVP

Table 2.2: FG124 aggregation lifetime and lag time with varying pH. Each condition run with 6 replicates in PTB buffer. Errors are standard errors of the mean.

pH	Lifetime τ (hr)	Lag time T_ℓ (hr)
5	0.34 ± 0.09	6.8 ± 0.1
6	0.35 ± 0.12	6.2 ± 0.2
7	0.38 ± 0.14	6.8 ± 0.4
8	0.50 ± 0.14	6.6 ± 0.2

Figure 2.4: Aggregation rates and lag times for varying PEG and PVP concentrations. Error bars are standard error of the mean.



condition decreased.

It is possible that the differences in aggregation time between PEG and PVP come from changes in viscosity. The two samples do have widely different viscosity, as measured by Steve Whitten. A 13% PEG solution in PTB has a dynamic viscosity of 15.87 mPa s, while that of a 13% PVP solution in PTB is 7.34 mPa s. Studies on aggregation of insulin or α synuclein show varying effects of viscosity. Increasing viscosity has been shown to increase the lag time and decrease the aggregation rate [113, 114]. However, other studies suggest that the behavior is nonmonotonic depending on viscosity and the aggregation propensity of the protein [112, 123]. While 13% PEG and PVP solutions have significantly different viscosities, both fall into what Munishkina et al. define as the “high concentration” regime where fibrillation rate is expected to decrease [123]. The trends shown in Fig. 2.4 roughly agree with the supposition that crowding effects decrease lag time and increase rate for moderate crowder concentrations but have the opposite effect as viscosity effects begin to dominate.

To further probe the origin of the differences in aggregation, we recorded NMR spectra for FSFG and fluorescence spectra for FG124 and FSFG in crowded PEG and PVP solutions.

2.2 Fluorescence spectra

An obvious structural difference between PEG and PVP as inert crowders is the presence of an aromatic ring in PVP (Fig. 2.5). The phenylalanines of FG124 also possess an aromatic ring, making ring-stacking or other interactions with PVP more likely. As the phenylalanines are also key to transport factor binding, it is important to understand their interactions with crowders. The presence of the ring itself makes fluorescence spectroscopy a natural choice for probing the differences between PEG and PVP as crowders. While protein fluorescence is typically dominated by tryptophan and then tyrosine fluorescence, these amino acids are absent from both FG124 and FSFG, leaving phenylalanine with the strongest fluorescent signal. Fluorescence spectra were therefore collected near phenylalanine’s emission maximum from both fresh and aggregated FG124 in PEG or PVP.

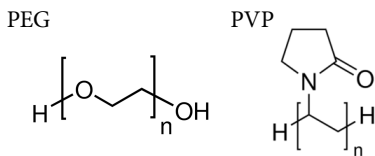


Figure 2.5: Chemical structures of PEG and PVP (Sigma).

2.2.1 Methods

2.2.1.1 Sample preparation

FG124 was purified as described above and in Appendix ?? and stored in PTB with 7M GuHCl. Immediately before use, 130 μL of 520 μM FG124 was desalted with a Zeba spin desalting column to remove the GuHCl. The resulting stock was used in the crowder samples, which had a final concentration of 340 μM FG124.

2.2.1.2 Fluorescence spectra

Fluorescence spectra were recorded using a Photon Technology International QM-6 fluorimeter. High concentrations of crowder were not possible due to background fluorescence, so samples containing 340 μM FG124 along with 5% w/v PEG or PVP were tested, along with FG124 in PTB only. Blanks consisting of crowder only, buffer only, water, and FSFG in buffer were measured as well. FG124 samples were tested before aggregation (within two hours of GuHCl removal), allowed to incubate at room temperature overnight without shaking, and tested again after aggregation. FG124 samples were visibly cloudy after overnight incubation.

A micro quartz UV cuvette with approximately 12 μL sample volume was used for all spectra. Between runs, the cuvette was rinsed three times with ethanol and five times with deionized water, and the exterior gently blotted with ethanol. When aggregated FG124 was used, it was necessary to first rinse the cuvette with 7M GuHCl, soak in 7M GuHCl for five minutes, and then follow the cleaning procedure above.

The fluorimeter was set to 4 nm excitation and emission slits and an excitation wavelength of 240 nm. Emission spectra were recorded at 1 nm intervals and automatically averaged over two runs. The PMT detector was set to 1000 V.

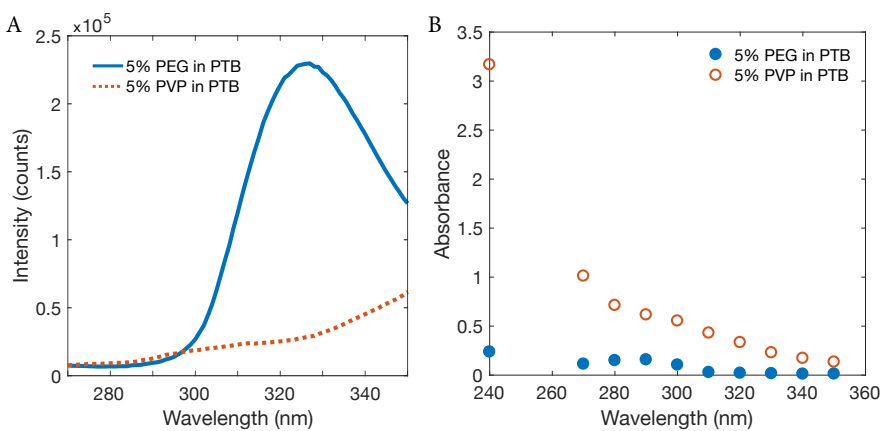


Figure 2.6: (A) Fluorescence spectrum of 5% w/v PEG and 5% w/v PVP in PTB. Normalized by subtracting PTB spectrum. (B) Absorbance spectrum of same samples. Measured on a (lookup old spectrophotometer) in a cuvette with working distance (lookup/estimate). Normalized by subtracting PTB absorbance.

2.2.1.3 Data processing

Data were normalized by averaging over two separate spectra and subtracting the appropriate blank spectrum containing the relevant crowder and buffer but no protein.

2.2.2 Results

Unfortunately, both PEG and PVP presented obstacles to the collection of UV fluorescence spectra. As shown in Fig. 2.6A, PEG displayed a prominent fluorescence peak centered at 320 nm. This may have been due to impurities in the PEG source (lookupL did I ever try better PEG). At low PEG concentrations, this peak was still small compared to that of FG124 (Fig. 2.8B) and could be subtracted from the signal. However, the PEG peak limited the maximum concentration of crowder to 5%. PVP, on the contrary, did not display a large peak within the region of interest, but its absorbance is quite high from 240-280 nm (Fig. 2.6B). The high PEG absorbance suppresses the fluorescence signal from FG124 (Fig. 2.8C). While more dramatic effects on the FG124 spectrum might be expected from higher concentrations, the limit of 5% w/v does serve to minimize any viscosity effects.

Figure 2.7 compares the phenylalanine peaks in FSFG concat-1, fresh and aggregated FG124, and pure phenylalanine in water from [124]. The phenylalanine peak slightly shifts toward longer wavelengths as the data progress from pure phenylalanine to FSFG to fresh and aggregated FG124. Additionally, a shoulder develops at longer wavelengths.

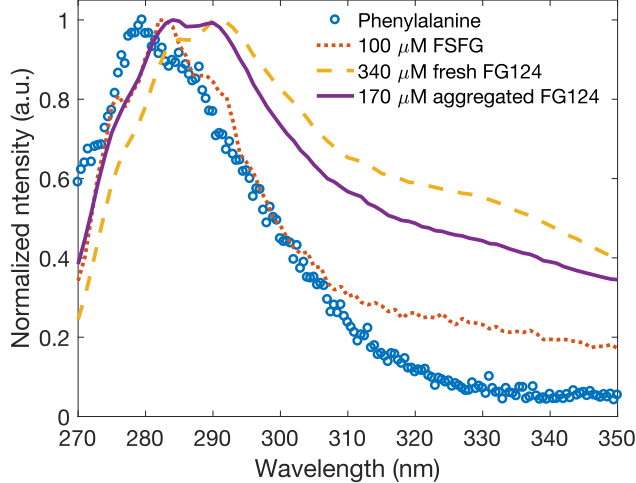


Figure 2.7: Fluorescence spectra of FSFG, FG124, and pure phenylalanine in water [124]. Excitation wavelength is 240 nm for all samples. Buffer spectra are subtracted (from FSFG and FG124 traces) and the resulting data is normalized to a maximum of one.

Fresh and aggregated FG124 samples are compared in Figs. 2.8 and 2.9. The PEG sample showed the largest difference upon aggregation, both in peak height and location. In both crowder conditions, but not in the buffer condition, a small peak appears in the aggregated FG124 near 310 nm.

2.2.3 Discussion

The fluorescence spectra of proteins can in principle be used to extract many types of information, from the properties of the environment in which its aromatic residues are located to protein folding and ligand binding [125]. This information comes from the many electronic states of the aromatic rings, which are often sensitive to the local environment and whose changes can cause shifts in fluorescence spectra. Of the three aromatic residues, tryptophan, with its double ring, dominates a protein's fluorescence, followed by tyrosine. Phenylalanine fluorescence is only measurable in the uncommon proteins which contain neither tryptophan or tyrosine. Fortunately, FSFG and FG124 contain no aromatic residues except for phenylalanine. The importance of those phenylalanine residues to binding both transport factors and other FG repeats makes them an appealing target for study by fluorimetry.

Given the rarity of detectable phenylalanine fluorescence in proteins, little literature exists interpreting its spectral shifts. That being the case, we can make an analogy to the tryptophan

Figure 2.8: Fluorescence spectra of fresh and aggregated FG124 in crowded conditions: (A) PTB buffer only, (B) 5% w/v PEG, (C) 5% w/v PVP. All data normalized by subtracting appropriate blank.

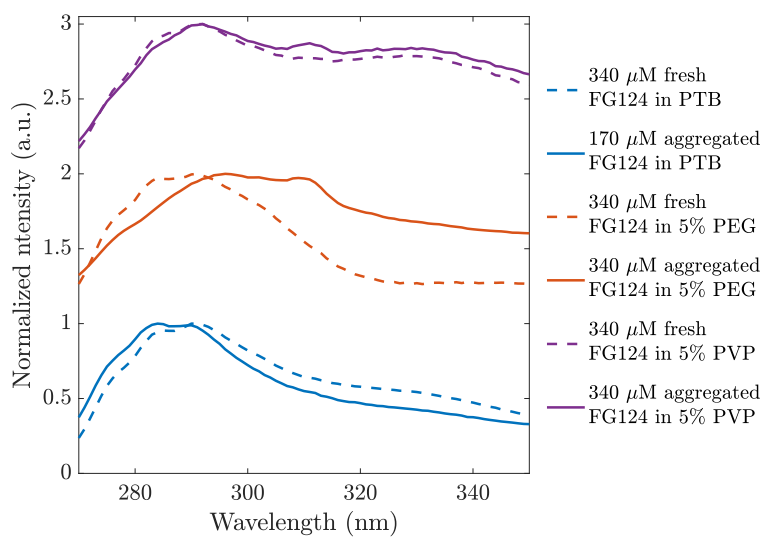
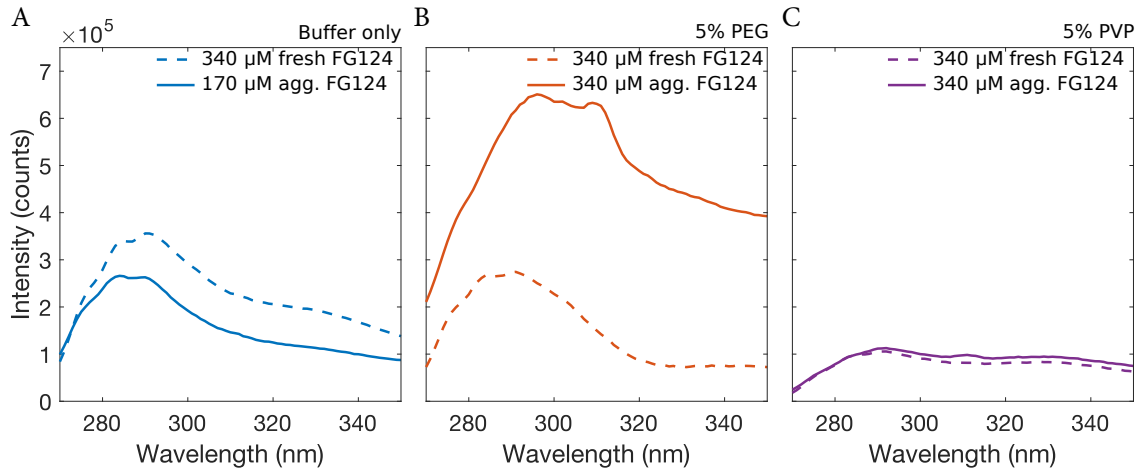


Figure 2.9: FG124 fluorescence comparison between 5% w/v PEG, 5% w/v PVP, and no crowder. All data normalized by subtracting appropriate blank and the resulting data is normalized to a maximum of one. Traces are offset for visual clarity.

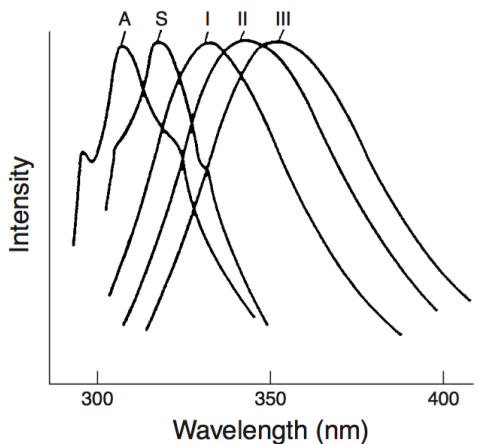


Figure 2.10: Qualitative depiction of spectral classes of tryptophan fluorescence. The classes correspond to differing solvent environments, with more hydrophilic environments generally being redshifted. Figure from [125].

literature in broad strokes. The complex electronic states of tryptophan give rise to a number of designated spectral classes, as shown in Fig. 2.10. While very few proteins display any one of these classes in their pure form, the major trend is that the spectrum becomes redshifted when the tryptophan residue is surrounded by an increasingly hydrophilic environment [125, 126]. It is not clear that a similar shift should hold true in detail for phenylalanine, but it seems likely that changes in local chemical environment could lead to shifts in its emission spectrum as well. The emergence of the smaller redshifted peaks in the spectra of the aggregated FSFG in crowded conditions, but not in the buffer sample (Fig. 2.9), could well mean that the phenylalanines are interacting differently with the crowding agents. In order to further investigate differences in the environment of the phenylalanines in crowded environments, we next measured their relaxation rates using NMR.

2.3 NMR relaxation measurements

NMR uses the magnetic relaxation of unpaired spins, found in atoms such as ^1H , ^{15}N , and ^{13}C to probe the local chemical environment of those spins. When applied to isotopically labeled proteins, NMR can provide information on protein-protein interactions, structure, and relaxation rates. Measurements of the longitudinal (R_1) and transverse (R_2) relaxation rates of each residue give information about the relaxation of individual spins and the time for the collection of spins in a sample to go out of phase with each other, respectively. In particular, R_2 increases when a

residue is interacting strongly with its environment.

Kathryn Wall measured the relaxation rates of FSFG in 13% w/v PEG or PVP. While ideally FG124 would be used, its propensity towards aggregation makes NMR experiments, which take several hours at a minimum, impossible. Despite its differences in aggregation behavior, FSFG is a useful proxy in this case. FSFG and FG124 are of similar lengths, derived from the Nup Nsp1, and contain similar number of FG motifs (6 FSFG motifs and 8 varied FG motifs, respectively) (Appendix ??). Given that we expect the crowders to particularly affect the phenylalanines, results from FSFG are likely a good estimate of FG124 behavior as well.

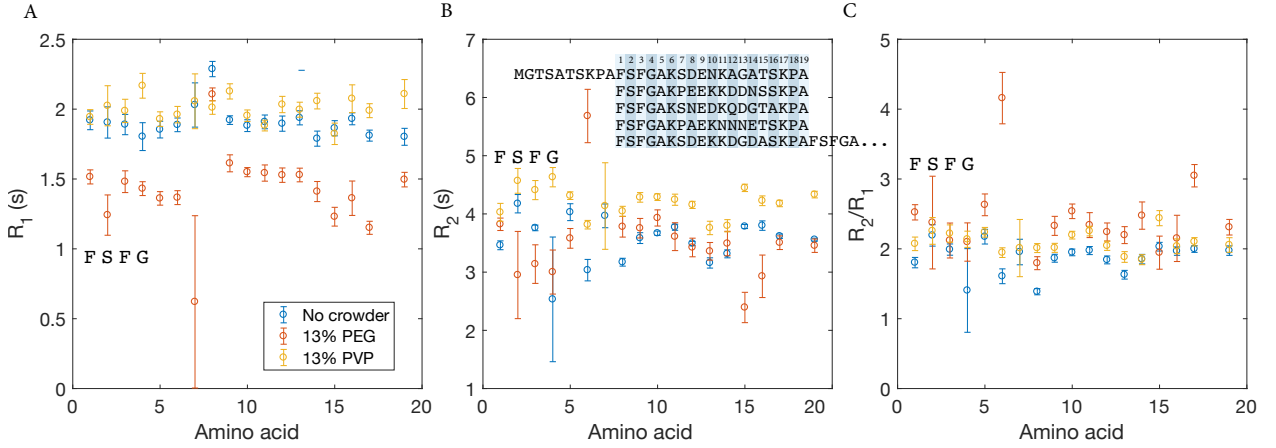
2.3.1 Methods

Isotopically-labeled, his-tagged ¹⁵N FSFG was expressed in BL21DE3 Gold cells in the pRSF plasmid (Kan resistant). Cells were grown in 1 L LB after inoculation with 1:500 preculture until reaching an OD₆₀₀ of 0.6-0.8. Cells were then pelleted by centrifuging for 10 minutes at 4000g and resuspended in a total of 1 L M9 salts pH 7.4 (10x M9 salts: 62 g/L Na₂HPO₄, 30 g/L KH₂PO₄, 5 g/L NaCl). After washing, cells were pelleted, resuspended in 1 L M9 minimal media with ¹⁵N ammonium chloride, and induced with 1 mM IPTG for 2-4 hours. The periplasmic matrix was then removed and the FSFG purified as described in Appendix ??.

The NMR samples contained 13% w/v of either PEG or PVP, 140 μM FSFG ¹⁵N, 10% D₂O, 1% 15 mM TSP, and 1%, 1mM DSS in PTB. Total sample volume was 336 μL. Ideally the protein concentration would have been at least 300 μM, but the presence of the crowders reduced the available volume for protein. An identical sample containing no crowders was also prepared.

NMR experiments were run by Kathryn Wall on an Inova 600 MHz. Using the standard ¹⁵N-HSQC experiment from the Varian BioPac, the parameter relaxT was adjusted for the measurement of *T*₁ and *T*₂ relaxation parameters. For measurement of *T*₁, relaxT was arrayed (0, 0.1, 0.2, 0.3, 0.4, 0.5, 0.6, 0.7, 0.8, 0.9 ms). For the measurement of *T*₂, relaxT was arrayed (0.01, 0.03, 0.05, 0.07, 0.09, 0.11, 0.13, 0.15, 0.17, 0.19, 0.21, 0.23, 0.25 ms). The data was processed using standard scripts in NMRPipe, and analyzed using CCPNmr Analysis software.

Figure 2.11: Relaxation rates for FSFG in 13% PEG, 13% PVP, or PTB only. The 19-amino-acid quasi-repeating unit that begins with the FSFG motif has been averaged over the first five repeats as shown. Experiments performed by Kathryn Wall. (A) Longitudinal relaxation rate R_1 , (B) transverse relaxation rate R_2 , (C) Ratio R_2/R_1 .



2.3.2 Results

Figure 2.11 shows the relaxation rates R_1 and R_2 of FSFG in 13% PEG, 13% PVP, or PTB without a crowder, along with the ratio R_2/R_1 . Due to the disordered nature of FSFG, many peaks in the NMR spectra overlap. Amino acids of the same type experience less difference in their average local chemical environment than they would in an ordered protein, with the result that a single peak often corresponds to several amino acids. This effect is particularly pronounced for the FSFG motif itself, in which the six repeated motifs are almost entirely collapsed to four peaks, one for each residue of the sequence. The sole exception is the phenylalanine closest to the N-terminal, which has a peak distinct from the others. Therefore, we broke the sequence of the FSFG peptide into quasi-repeating segments, each 19 amino acids in length, which begin with an FSFG motif and contain the hydrophilic linker which separates it from the next FSFG (Fig. 2.11B, inset). The errors in R_1 and R_2 are given by the weighted average of the fit errors for the unique peaks that are being averaged [127]. The errors of the ratio R_2/R_1 were propagated from R_1 and R_2 errors.

There are noticeable differences between the crowded conditions and buffer condition, which are likely due to a combination of viscosity effects and differences in interactions with the crowders.

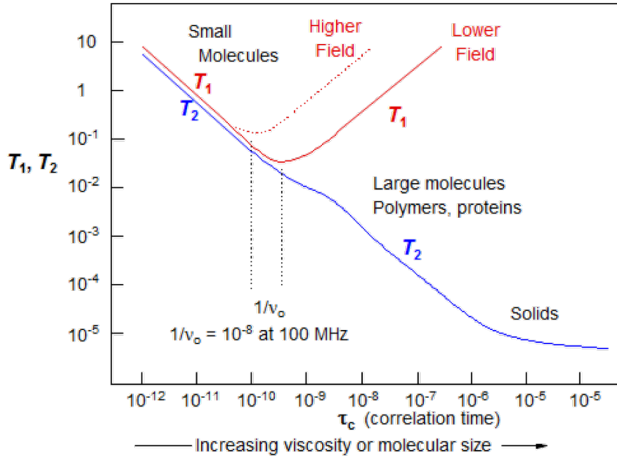


Figure 2.12: Approximate dependence of relaxation times T_1 and T_2 on solvent viscosity. Figure from [128].

Surprisingly, the systemic differences in rates do not all correspond to viscosity changes. For example, the PVP sample has the highest R_1 and R_2 values overall, despite having an intermediate viscosity. The R_1 values are significantly lower for the PEG sample than the other two, which also is not obviously explained by viscosity changes.

2.3.3 Discussion

There are noticeable differences between the relaxation rates in 13% PEG, 13% PVP, and without crowders whose source is not obvious. In addition to varying the crowding agent, the viscosity varies from sample to sample, with buffer having the lowest and PEG the highest viscosity. Some differences in the rates are likely due to the change in viscosity, while others may be due to differences in the peptide's interaction with the crowders. As mentioned above, PVP shows the highest relaxation rates overall despite having an intermediate viscosity. On the other hand, the ratio R_2/R_1 generally shows higher rates for PEG, then for PVP, with the lowest rates belonging to the buffer-only sample.

The typical behavior of relaxation times (with $T_1 = 1/R_1$ and $T_2 = 1/R_2$) as a function of viscosity is shown in Fig. 2.12 [128]. As viscosity increases, the transverse relaxation time T_2 decreases monotonically. However, the longitudinal relaxation time T_1 begins by decreasing, reaches a turnaround point, and increases afterwards. The location of the turnaround point τ_0 is related to the strength of the NMR magnetic field expressed as a frequency ν_0 by $\tau_0 = 1/\nu_0$. For the 600

MHz instrument used in these experiments, $\tau_0 \approx 1 \times 10^{-9}$ s. (Am I getting this right?) Given that the measured rates are on the order of 1 s, T_1 is likely in the region where it should decrease with increasing viscosity. In addition, the viscosities span an order of magnitude from buffer (1 mP s) to 13% PEG (15 mP s), and would be expected to produce a comparably large change in relaxation rates. Instead, the rates change by approximately 25% at most, and the PEG sample shows the lowest relaxation rates and therefore the largest relaxation times. Overall, the relaxation rates show features that are not obviously explained by changes in sample viscosity and may be due to differences in their interactions with the crowding agents.

2.4 Conclusions

We used several methods to investigate FG Nup aggregation in crowded conditions, focusing on FG124 as a representative peptide. All methods indicate that there are indeed differences in aggregation and the resulting chemical environments depending on the presence and type of crowder. The aggregation timecourses pointed to differences between most of the crowders tested, and between PEG and PVP in particular. Since PEG and PVP are often used interchangeably as inert crowders, we pursued these differences using fluorimetry and NMR. Both reinforced the idea that there are in fact differences between FG124 behavior in these crowders. The fluorescence spectra of the aggregated FG124 in particular suggests that the phenylalanines behave differently in crowded conditions than in buffer only. Since FG repeats are involved not only to binding transport factors for selective transport, but also in forming transient crosslinks with other FG Nups, our results indicate that great care should be taken in determining what conditions to use to study Nups *in vitro*.

Chapter 3

Conclusions and future directions

Living systems contain many examples of selective filters which control the transport of all manner of macromolecules. In this work, we studied biofilters which allow rapid transport of highly specific targets, counterintuitively relying on binding interactions to promote rather than hinder flux. These filters often contain similar features, such as transient, multivalent binding and binding to flexible, dynamic tethers. In order to understand the presence of these features, we approached the problem through both modeling and experiment. Bound-state diffusion proved to be a key parameter for selectivity. While the theory and experimental setup were based on nuclear transport, they were not designed to exactly reproduce the nuclear pore, but to be applicable to a wider variety of biofilters.

We created a minimal model of the nuclear pore, containing very little beyond the diffusion of transport factors and their binding to FG Nups. Interestingly, even this highly simplified model was able to reproduce the selectivity properties of the nuclear pore, predicting that binding could increase the flux of a protein through this material up to 300-fold over the flux of an identical inert protein. The simplicity of our model made the key parameter clear: we could not reproduce the selectivity of the nuclear pore without allowing bound-state diffusion, that is, assuming that bound Nup - transport factor complexes were mobile within the pore. Plausible mechanisms of bound diffusion in the nuclear pore include tethered diffusion arising from the disordered, flexible nature of the Nups, and inter-chain hopping of the transport factor due to its binding multivalency.

We modeled both of these mechanisms and found that they allow for significant bound mobility and therefore high selectivity. These mechanisms may also be at work in other highly-specific, high-throughput biofilters.

After developing the minimal model of selectivity, we began developing a synthetic biofilter inspired by the nuclear pore with which to experimentally probe the effect of bound-state diffusion on selectivity. In order to capture the key features of selectivity, we designed hydrogels containing peptide tethers derived from FG Nups. The transport factor NTF2 served as a test protein whose diffusion we could compare with a similarly-size but nonbinding counterpart. Fluorescence recovery after photobleaching (FRAP) was used to determine the effective diffusion constants of both NTF2 and an inert protein, from which the bound diffusion constant was calculated. We measured a non-zero bound diffusion constant that is consistent with the predictions of our model, and tested the effect of varying Nup length on bound-state diffusion.

Additionally, we probed the aggregation behavior of an FG-Nup-derived peptide in several crowded conditions. We used a fluorescent aggregation assay as well as NMR and fluorimetry to investigate differences in the aggregated state between crowding conditions, and found that even inert crowders which are widely used interchangeably show differences in the local chemical environments of the peptide.

Although a true hydrogel-based selective biofilter proved challenging to design, our nuclear-pore-inspired material can be used to measure the bound-state diffusion of proteins. This parameter is likely important to a variety of problems involving rapid transport of highly-selective proteins. The model and biomaterials developed here could be used to investigate these systems more generally in the future. This work suggests that bound-state diffusion, particularly when resulting from transient, multivalent binding, may help explain a number of unusual biological filters.

3.1 Future directions

It would be interesting to apply our model of bound-state diffusion to other selective biofilters, particularly those, like the ones described in Chapter ??, which share similarities with the nuclear

pore. One question which we are well-positioned to investigate using both our theoretical model and experimental setup is particle diffusion in mucus [75,81]. As described in Sec. 1.2.1, the mucus barrier in the lungs is an obstacle to drug delivery, because nanoparticles tend to get trapped in this barrier, which is constantly being cleared and replaced. Our bound-state diffusion model of flux through a barrier could be used to describe the situation of nanoparticles which interact with the mucus layer, particularly if we modify it to include a mucus flux representing the clearance of mucus. It is currently not clear whether drug delivery is better accomplished with particles designed to bind to mucins or to avoid interactions [74,77]. Our model broadly predicts that the flux of nanoparticles through the mucus layer will be higher with binding but only if the binding mechanism permits high mobility of the bound complex. A first step towards testing our model is measuring the diffusion of nanoparticles in mucus, an experiment that could be done using the flow chambers developed in Chapter ???. It would likely be possible to use both the model and experimental systems with only minor modifications to investigate nanoparticle diffusion and drug delivery through mucus barriers.

Another system with striking similarities to our bound-diffusion model of selectivity is the speed-stability paradox of transcription factor and DNA damage repair proteins that target specific sites on DNA (Sec. 1.2.2). In the case of the DNA damage repair protein poly(ADP-ribose) polymerase 1 (PARP1) in particular, PARP1 binds even intact chromatin with micromolar affinity, but it moves to the sites of DNA damage with a diffusion constant only an order of magnitude less than its diffusion in water [94,95]. If there is truly only negligible free PARP1 in the nucleus, and it is almost entirely bound to DNA, then all diffusion to sites of damage must be bound diffusion. Given the high diffusion constant measured, we might then expect to see evidence of the mechanisms which we think give rise to bound diffusion in the nuclear pore complex: multivalent binding and tethered diffusion.

Indeed, PARP1 contains four DNA binding domains and has been shown to possess a “hopping” mechanism to move between stands while bound [94]. Furthermore, recent unpublished data from Johannes Rudolph and the Luger group suggest that PARP1 may dimerize while bound to

intact DNA searching for damage. Previous work has also indicated that PARP1 may dimerize, though the context and extent of dimerization is unclear [129, 130]. At first glance, our model predicts that dimerization could increase the bound diffusion constant, provided it increases the rate of hopping between strands. Multivalent binding appears to be important to PARP1 diffusion in several ways. Tethered diffusion is also a plausible mechanism in this case, as there is evidence that chromatin is dynamic and could act as a flexible tether [131, 132]. Naive calculations which use only our tethered diffusion model and do not allow hopping are consistent with the calculated off-rate from intact DNA (Sec ??).

Finally, it is interesting that PARP1 binding to DNA is another example of a highly multivalent system, with several binding sites on each PARP1 and many on each DNA strand, for which *in vivo* affinity measurements are very difficult. Even affinity measurements to intact DNA as opposed to damaged are difficult to carry out *in vitro*, as most DNA *in vitro* is damaged somehow. This situation reminds me of the similar historical difficulty in measuring Nup - transport factor affinities, and the way that the field's understanding of the mechanisms of nuclear transport evolved as those measured values improved. If the problem of binding affinity in the nuclear pore is any indication, I would not be surprised to find that future calculations of PARP1's affinity for intact DNA show weaker binding than is currently accepted.

The similarities between the nuclear pore and PARP1 diffusion are fascinating, as is the problem of diffusion through a mucus barrier, and our model of selectivity is well-positioned to offer insight into all of these. While ideas of bound-state diffusion are already present in all of these fields, I think our model has particular value in clarifying why bound-state diffusion can lead to unusual selective filters and in suggesting practical mechanisms with which to engineer systems with bound diffusion. There are a surprising number of examples of selective biofilters which use binding to increase flux, and our model provides new insight into how they might accomplish this remarkable task.

Bibliography

- [1] B. L. Timney, B. Raveh, R. Mironksa, J. M. Trivedi, S. J. Kim, D. Russel, S. R. Wente, A. Sali, and M. P. Rout. Simple rules for passive diffusion through the nuclear pore complex. *J Cell Biol*, 215(1):57–76, October 2016.
- [2] V. N. Uversky. A decade and a half of protein intrinsic disorder: Biology still waits for physics. *Protein Science*, 22(6):693–+, June 2013. WOS:000319422500001.
- [3] P. E. Wright and H. J. Dyson. Intrinsically disordered proteins in cellular signalling and regulation. *Nature Reviews Molecular Cell Biology*, 16(1):18–29, January 2015.
- [4] I. V. Aramburu and E. A. Lemke. Floppy but not sloppy: Interaction mechanism of FG-nucleoporins and nuclear transport receptors. *Seminars in Cell & Developmental Biology*, 68:34–41, August 2017.
- [5] M. M. Babu, R. van der Lee, N. S. de Groot, and J. Gsponer. Intrinsically disordered proteins: Regulation and disease. *Current Opinion in Structural Biology*, 21(3):432–440, June 2011.
- [6] C. P. Brangwynne, P. Tompa, and R. V. Pappu. Polymer physics of intracellular phase transitions. *Nature Physics*, 11(11):899–904, November 2015.
- [7] M. Beck and E. Hurt. The nuclear pore complex: Understanding its function through structural insight. *Nature Reviews Molecular Cell Biology*, 18(2):73–89, February 2017.
- [8] S. S. Patel, B. J. Belmont, J. M. Sante, and M. F. Rexach. Natively Unfolded Nucleoporins Gate Protein Diffusion across the Nuclear Pore Complex. *Cell*, 129(1):83–96, April 2007.
- [9] C. Strambio-De-Castillia, M. Niepel, and M. P. Rout. The nuclear pore complex: Bridging nuclear transport and gene regulation. *Nature Reviews Molecular Cell Biology*, 11(7):490–501, July 2010.
- [10] L. J. Terry and S. R. Wente. Flexible Gates: Dynamic Topologies and Functions for FG-Nucleoporins in Nucleocytoplasmic Transport. *Eukaryotic Cell*, 8(12):1814–1827, December 2009.
- [11] L. E. Hough, K. Dutta, S. Sparks, D. B. Temel, A. Kamal, J. Tetenbaum-Novatt, M. P. Rout, and D. Cowburn. The molecular mechanism of nuclear transport revealed by atomic-scale measurements. *eLife*, 4:e10027, September 2015.

- [12] Y. Sakiyama, A. Mazur, L. E. Kapinos, and R. Y. H. Lim. Spatiotemporal dynamics of the nuclear pore complex transport barrier resolved by high-speed atomic force microscopy. *Nature Nanotechnology*, 11(8):719–723, August 2016.
- [13] L.-C. Tu and S. M. Musser. Single Molecule Studies of Nucleocytoplasmic Transport. *Biochimica et biophysica acta*, 1813(9):1607–1618, September 2011.
- [14] R. Moussavi-Baygi and M. R. K. Mofrad. Rapid Brownian Motion Primes Ultrafast Reconstruction of Intrinsically Disordered Phe-Gly Repeats Inside the Nuclear Pore Complex. *Scientific Reports*, 6, July 2016.
- [15] R. L. Schoch, L. E. Kapinos, and R. Y. H. Lim. Nuclear transport receptor binding avidity triggers a self-healing collapse transition in FG-nucleoporin molecular brushes. *Proceedings of the National Academy of Sciences of the United States of America*, 109(42):16911–16916, October 2012.
- [16] J. Yamada, J. L. Phillips, S. Patel, G. Goldfien, A. Calestagne-Morelli, H. Huang, R. Reza, J. Acheson, V. V. Krishnan, S. Newsam, A. Gopinathan, E. Y. Lau, M. E. Colvin, V. N. Uversky, and M. F. Rexach. A bimodal distribution of two distinct categories of intrinsically disordered structures with separate functions in FG nucleoporins. *Molecular & cellular proteomics: MCP*, 9(10):2205–2224, October 2010.
- [17] D. Ando, R. Zandi, Y. W. Kim, M. Colvin, M. Rexach, and A. Gopinathan. Nuclear Pore Complex Protein Sequences Determine Overall Copolymer Brush Structure and Function. *Biophysical Journal*, 106(9):1997–2007, May 2014.
- [18] M. Tagliazucchi, O. Peleg, M. Kroeger, Y. Rabin, and I. Szleifer. Effect of charge, hydrophobicity, and sequence of nucleoporins on the translocation of model particles through the nuclear pore complex. *Proceedings of the National Academy of Sciences of the United States of America*, 110(9):3363–3368, February 2013. WOS:000315841900039.
- [19] B. Zeitler and K. Weis. The FG-repeat asymmetry of the nuclear pore complex is dispensable for bulk nucleocytoplasmic transport *in vivo*. *The Journal of Cell Biology*, 167(4):583–590, November 2004.
- [20] L. A. Strawn, T. Shen, N. Shulga, D. S. Goldfarb, and S. R. Wente. Minimal nuclear pore complexes define FG repeat domains essential for transport. *Nature Cell Biology*, 6(3):197–206, March 2004.
- [21] S. W. Kowalczyk, L. Kapinos, T. R. Blosser, T. Magalhães, P. van Nies, R. Y. H. Lim, and C. Dekker. Single-molecule transport across an individual biomimetic nuclear pore complex. *Nature Nanotechnology*, 6(7):433–438, July 2011.
- [22] T. Jovanovic-Talisman, J. Tetenbaum-Novatt, A. S. McKenney, A. Zilman, R. Peters, M. P. Rout, and B. T. Chait. Artificial nanopores that mimic the transport selectivity of the nuclear pore complex. *Nature*, 457(7232):1023–1027, February 2009.
- [23] B. Pyhtila and M. Rexach. A Gradient of Affinity for the Karyopherin Kap95p along the Yeast Nuclear Pore Complex. *Journal of Biological Chemistry*, 278(43):42699–42709, October 2003.

- [24] D. Gilchrist, B. Mykytka, and M. Rexach. Accelerating the Rate of Disassembly of Karyopherin-Cargo Complexes. *Journal of Biological Chemistry*, 277(20):18161–18172, May 2002.
- [25] J. Tetenbaum-Novatt, L. E. Hough, R. Mironcka, A. S. McKenney, and M. P. Rout. Nucleocytoplasmic Transport: A Role for Nonspecific Competition in Karyopherin-Nucleoporin Interactions. *Molecular & Cellular Proteomics : MCP*, 11(5):31–46, May 2012.
- [26] S. Milles, D. Mercadante, I. V. Aramburu, M. R. Jensen, N. Banterle, C. Koehler, S. Tyagi, J. Clarke, S. L. Shammas, M. Blackledge, F. Gräter, and E. A. Lemke. Plasticity of an Ultrafast Interaction between Nucleoporins and Nuclear Transport Receptors. *Cell*, 163(3):734–745, October 2015.
- [27] R. Hayama, S. Sparks, L. M. Hecht, K. Dutta, J. M. Karp, C. M. Cabana, M. P. Rout, and D. Cowburn. Thermodynamic characterization of the multivalent interactions underlying rapid and selective translocation through the nuclear pore complex. *Journal of Biological Chemistry*, 293(12):4555–4563, 2018.
- [28] T. Jovanovic-Talisman and A. Zilman. Protein Transport by the Nuclear Pore Complex: Simple Biophysics of a Complex Biomachine. *Biophysical Journal*, 113(1):6–14, July 2017.
- [29] L. E. Kapinos, B. Huang, C. Rencurel, and R. Y. H. Lim. Karyopherins regulate nuclear pore complex barrier and transport function. *J Cell Biol*, page jcb.201702092, September 2017.
- [30] S. H. Yoshimura and T. Hirano. HEAT repeats – versatile arrays of amphiphilic helices working in crowded environments? *J Cell Sci*, 129(21):3963–3970, November 2016.
- [31] Y. M. Chook and K. E. Süel. Nuclear import by karyopherin-*Bs*: Recognition and inhibition. *Biochimica et Biophysica Acta (BBA) - Molecular Cell Research*, 1813(9):1593–1606, September 2011.
- [32] L. E. Kapinos, R. L. Schoch, R. S. Wagner, K. D. Schleicher, and R. Y. H. Lim. Karyopherin-Centric Control of Nuclear Pores Based on Molecular Occupancy and Kinetic Analysis of Multivalent Binding with FG Nucleoporins. *Biophysical Journal*, 115(12):2512, December 2018.
- [33] K. D. Schleicher, S. L. Dettmer, L. E. Kapinos, S. Pagliara, U. F. Keyser, S. Jeney, and R. Y. H. Lim. Selective transport control on molecular velcro made from intrinsically disordered proteins. *Nature Nanotechnology*, 9(7):525–530, July 2014.
- [34] L. E. Kapinos, R. L. Schoch, R. S. Wagner, K. D. Schleicher, and R. Y. Lim. Karyopherin-Centric Control of Nuclear Pores Based on Molecular Occupancy and Kinetic Analysis of Multivalent Binding with FG Nucleoporins. *Biophysical Journal*, 106(8):1751–1762, April 2014.
- [35] D. Görlich, N. Panté, U. Kutay, U. Aebi, and F. R. Bischoff. Identification of different roles for RanGDP and RanGTP in nuclear protein import. *The EMBO Journal*, 15(20):5584–5594, October 1996.
- [36] M. Stewart. Molecular mechanism of the nuclear protein import cycle. *Nature Reviews. Molecular Cell Biology*, 8(3):195–208, March 2007.

- [37] K. Ribbeck, G. Lipowsky, H. M. Kent, M. Stewart, and D. Görlich. NTF2 mediates nuclear import of Ran. *The EMBO Journal*, 17(22):6587–6598, November 1998.
- [38] R. Bayliss, K. Ribbeck, D. Akin, H. M. Kent, C. M. Feldherr, D. Görlich, and M. Stewart. Interaction between NTF2 and xFxFG-containing nucleoporins is required to mediate nuclear import of RanGDP 1. *Journal of Molecular Biology*, 293(3):579–593, October 1999.
- [39] K. Ribbeck and D. Görlich. Kinetic analysis of translocation through nuclear pore complexes. *The EMBO Journal*, 20(6):1320–1330, March 2001.
- [40] J. P. Siebrasse and R. Peters. Rapid translocation of NTF2 through the nuclear pore of isolated nuclei and nuclear envelopes. *EMBO Reports*, 3(9):887–892, September 2002.
- [41] N. I. Kiskin, J. P. Siebrasse, and R. Peters. Optical Micowell Assay of Membrane Transport Kinetics. *Biophysical Journal*, 85(4):2311–2322, October 2003.
- [42] G. J. Stanley, A. Fassati, and B. W. Hoogenboom. Biomechanics of the transport barrier in the nuclear pore complex. *Seminars in Cell & Developmental Biology*, 68:42–51, August 2017.
- [43] A. Paradise, M. K. Levin, G. Korza, and J. H. Carson. Significant proportions of nuclear transport proteins with reduced intracellular mobilities resolved by fluorescence correlation spectroscopy. *Journal of molecular biology*, 365(1):50–65, January 2007.
- [44] W. Yang and S. M. Musser. Nuclear import time and transport efficiency depend on importin β concentration. *The Journal of Cell Biology*, 174(7):951–961, September 2006.
- [45] T. Dange, D. Grünwald, A. Grünwald, R. Peters, and U. Kubitscheck. Autonomy and robustness of translocation through the nuclear pore complex: A single-molecule study. *The Journal of Cell Biology*, 183(1):77–86, 2008.
- [46] U. Kubitscheck, D. Grünwald, A. Hoekstra, D. Rohleider, T. Kues, J. P. Siebrasse, and R. Peters. Nuclear transport of single molecules. *The Journal of Cell Biology*, 168(2):233–243, January 2005.
- [47] M. Elbaum. Polymers in the Pore. *Science*, 314(5800):766–767, November 2006.
- [48] S. Frey, R. P. Richter, and D. Görlich. FG-Rich Repeats of Nuclear Pore Proteins Form a Three-Dimensional Meshwork with Hydrogel-Like Properties. *Science*, 314(5800):815–817, November 2006.
- [49] S. Frey and D. Görlich. A Saturated FG-Repeat Hydrogel Can Reproduce the Permeability Properties of Nuclear Pore Complexes. *Cell*, 130(3):512–523, August 2007.
- [50] C. Ader, S. Frey, W. Maas, H. B. Schmidt, D. Görlich, and M. Baldus. Amyloid-like interactions within nucleoporin FG hydrogels. *Proceedings of the National Academy of Sciences*, 107(14):6281–6285, June 2010.
- [51] M. Kim, W. G. Chen, J. W. Kang, M. J. Glassman, K. Ribbeck, and B. D. Olsen. Artificially Engineered Protein Hydrogels Adapted from the Nucleoporin Nsp1 for Selective Biomolecular Transport. *Advanced materials (Deerfield Beach, Fla.)*, 27(28):4207–4212, July 2015.

- [52] T. Bickel and R. Bruinsma. The Nuclear Pore Complex Mystery and Anomalous Diffusion in Reversible Gels. *Biophysical Journal*, 83(6):3079–3087, December 2002.
- [53] C. Gu, A. Vovk, T. Zheng, R. D. Coalson, and A. Zilman. The Role of Cohesiveness in the Permeability of the Spatial Assemblies of FG Nucleoporins. *Biophysical Journal*, 116(7):1204–1215, April 2019.
- [54] M. P. Rout, J. D. Aitchison, A. Suprapto, K. Hjertaas, Y. Zhao, and B. T. Chait. The Yeast Nuclear Pore Complex Composition, Architecture, and Transport Mechanism. *The Journal of Cell Biology*, 148(4):635–652, February 2000.
- [55] R. Y. H. Lim, U. Aebi, and B. Fahrenkrog. Towards reconciling structure and function in the nuclear pore complex. *Histochemistry and Cell Biology*, 129(2):105–116, February 2008.
- [56] R. S. Wagner, L. E. Kapinos, N. J. Marshall, M. Stewart, and R. Y. H. Lim. Promiscuous Binding of Karyopherin β 1 Modulates FG Nucleoporin Barrier Function and Expedites NTF2 Transport Kinetics. *Biophysical Journal*, 108(4):918–927, February 2015.
- [57] R. Zahn, D. Osmanović, S. Ehret, C. A. Callis, S. Frey, M. Stewart, C. You, D. Görlich, B. W. Hoogenboom, and R. P. Richter. A physical model describing the interaction of nuclear transport receptors with FG nucleoporin domain assemblies. *eLife*, 5:e14119, April 2016.
- [58] A. Vovk, C. Gu, M. G. Opferman, L. E. Kapinos, R. Y. Lim, R. D. Coalson, D. Jasnow, and A. Zilman. Simple biophysics underpins collective conformations of the intrinsically disordered proteins of the Nuclear Pore Complex. *eLife*, 5:e10785, May 2016.
- [59] A. E. Nasrabad, D. Jasnow, A. Zilman, and R. D. Coalson. Precise control of polymer coated nanopores by nanoparticle additives: Insights from computational modeling. *Journal of Chemical Physics*, 145(6):064901, August 2016. WOS:000381680300043.
- [60] J. S. Mincer and S. M. Simon. Simulations of nuclear pore transport yield mechanistic insights and quantitative predictions. *Proceedings of the National Academy of Sciences of the United States of America*, 108(31):E351–358, August 2011.
- [61] A. Zilman, S. D. Talia, B. T. Chait, M. P. Rout, and M. O. Magnasco. Efficiency, Selectivity, and Robustness of Nucleocytoplasmic Transport. *PLOS Computational Biology*, 3(7):e125, July 2007.
- [62] L.-C. Tu, G. Fu, A. Zilman, and S. M. Musser. Large cargo transport by nuclear pores: Implications for the spatial organization of FG-nucleoporins. *The EMBO journal*, 32(24):3220–3230, December 2013.
- [63] J. Tetenbaum-Novatt, L. E. Hough, R. Mironská, A. S. McKenney, and M. P. Rout. Nucleocytoplasmic Transport: A Role for Nonspecific Competition in Karyopherin-Nucleoporin Interactions. *Molecular & Cellular Proteomics : MCP*, 11(5):31–46, May 2012.
- [64] A. Zilman. Effects of Multiple Occupancy and Interparticle Interactions on Selective Transport through Narrow Channels: Theory versus Experiment. *Biophysical Journal*, 96(4):1235–1248, February 2009.

- [65] A. Zilman, S. D. Talia, T. Jovanovic-Talismann, B. T. Chait, M. P. Rout, and M. O. Magnasco. Enhancement of Transport Selectivity through Nano-Channels by Non-Specific Competition. *PLOS Computational Biology*, 6(6):e1000804, June 2010.
- [66] B. L. Timney, J. Tetenbaum-Novatt, D. S. Agate, R. Williams, W. Zhang, B. T. Chait, and M. P. Rout. Simple kinetic relationships and nonspecific competition govern nuclear import rates in vivo. *J Cell Biol*, 175(4):579–593, November 2006.
- [67] Y. J. Yang, D. J. Mai, T. J. Dursch, and B. D. Olsen. Nucleopore-Inspired Polymer Hydrogels for Selective Biomolecular Transport. *Biomacromolecules*, September 2018.
- [68] A. N. Ananth, A. Mishra, S. Frey, A. Dwarkasing, R. Versloot, E. van der Giessen, D. Görlich, P. Onck, and C. Dekker. Spatial structure of disordered proteins dictates conductance and selectivity in nuclear pore complex mimics. *eLife*, 7:e31510, February 2018.
- [69] S. Frey and D. Görlich. FG/FxFG as well as GLFG repeats form a selective permeability barrier with self-healing properties. *The EMBO Journal*, 28(17):2554–2567, September 2009.
- [70] A. K. Friedman and L. A. Baker. Synthetic hydrogel mimics of the nuclear pore complex display selectivity dependent on FG-repeat concentration and electrostatics. *Soft Matter*, 12(47):9477–9484, November 2016.
- [71] P. D. E. Fisher, Q. Shen, B. Akpinar, L. K. Davis, K. K. H. Chung, D. Baddeley, A. Saric, T. J. Melia, B. W. Hoogenboom, C. Lin, and C. P. Lusk. A Programmable DNA Origami Platform for Organizing Intrinsically Disordered Nucleoporins within Nanopore Confinement. *ACS nano*, January 2018.
- [72] T. Carlson, J. Lock, and R. Carrier. Engineering the Mucus Barrier. *Annual Review of Biomedical Engineering*, 20(1):197–220, 2018.
- [73] A. Popov, L. Schopf, J. Bourassa, and H. Chen. Enhanced pulmonary delivery of fluticasone propionate in rodents by mucus-penetrating nanoparticles. *International Journal of Pharmaceutics*, 502(1):188–197, April 2016.
- [74] A. F. L. Schneider and C. P. R. Hackenberger. Fluorescent labelling in living cells. *Current Opinion in Biotechnology*, 48:61–68, December 2017.
- [75] J. Witten and K. Ribbeck. The particle in the spider’s web: Transport through biological hydrogels. *Nanoscale*, May 2017.
- [76] S. K. Lai, Y.-Y. Wang, K. Hida, R. Cone, and J. Hanes. Nanoparticles reveal that human cervicovaginal mucus is riddled with pores larger than viruses. *Proceedings of the National Academy of Sciences*, 107(2):598–603, January 2010.
- [77] S. K. Lai, J. S. Suk, A. Pace, Y.-Y. Wang, M. Yang, O. Mert, J. Chen, J. Kim, and J. Hanes. Drug carrier nanoparticles that penetrate human chronic rhinosinusitis mucus. *Biomaterials*, 32(26):6285–6290, September 2011.
- [78] N. A. Peppas and P. A. Buri. Surface, interfacial and molecular aspects of polymer bioadhesion on soft tissues. *Journal of Controlled Release*, 2:257–275, November 1985.

- [79] Y. Shang, K. Inthavong, and J. Tu. Development of a computational fluid dynamics model for mucociliary clearance in the nasal cavity. *Journal of Biomechanics*, 85:74–83, March 2019.
- [80] J. C. Lay, M. R. Stang, P. E. Fisher, J. R. Yankaskas, and W. D. Bennett. Airway retention of materials of different solubility following local intrabronchial deposition in dogs. *Journal of Aerosol Medicine: The Official Journal of the International Society for Aerosols in Medicine*, 16(2):153–166, 2003.
- [81] J. M. Newby, I. Seim, M. Lysy, Y. Ling, J. Huckaby, S. K. Lai, and M. G. Forest. Technological strategies to estimate and control diffusive passage times through the mucus barrier in mucosal drug delivery. *Advanced Drug Delivery Reviews*, 124:64–81, January 2018.
- [82] X. Huang, J. Chisholm, J. Zhuang, Y. Xiao, G. Duncan, X. Chen, J. S. Suk, and J. Hanes. Protein nanocages that penetrate airway mucus and tumor tissue. *Proceedings of the National Academy of Sciences*, 114(32):E6595–E6602, August 2017.
- [83] P. Mastorakos, A. L. da Silva, J. Chisholm, E. Song, W. K. Choi, M. P. Boyle, M. M. Morales, J. Hanes, and J. S. Suk. Highly compacted biodegradable DNA nanoparticles capable of overcoming the mucus barrier for inhaled lung gene therapy. *Proceedings of the National Academy of Sciences*, 112(28):8720–8725, July 2015.
- [84] B. Porsio, E. F. Craparo, N. Mauro, G. Giammona, and G. Cavallaro. Mucus and Cell-Penetrating Nanoparticles Embedded in Nano-into-Micro Formulations for Pulmonary Delivery of Ivacaftor in Patients with Cystic Fibrosis. *ACS Applied Materials & Interfaces*, 10(1):165–181, January 2018.
- [85] B. C. Tang, M. Dawson, S. K. Lai, Y.-Y. Wang, J. S. Suk, M. Yang, P. Zeitlin, M. P. Boyle, J. Fu, and J. Hanes. Biodegradable polymer nanoparticles that rapidly penetrate the human mucus barrier. *Proceedings of the National Academy of Sciences of the United States of America*, 106(46):19268–19273, November 2009.
- [86] L. Mirny, M. Slutsky, Z. Wunderlich, A. Tafvizi, J. Leith, and A. Kosmrlj. How a protein searches for its site on DNA: The mechanism of facilitated diffusion. *Journal of Physics A: Mathematical and Theoretical*, 42(43):434013, October 2009.
- [87] J. Iwahara and Y. Levy. Speed-stability paradox in DNA-scanning by zinc-finger proteins. *Transcription*, 4(2):58–61, March 2013.
- [88] S. E. Halford. An end to 40 years of mistakes in DNA–protein association kinetics? *Biochemical Society Transactions*, 37(2):343–348, April 2009.
- [89] B. Raveh, J. M. Karp, S. Sparks, K. Dutta, M. P. Rout, A. Sali, and D. Cowburn. Slide-and-exchange mechanism for rapid and selective transport through the nuclear pore complex. *Proceedings of the National Academy of Sciences*, 113(18):E2489–E2497, May 2016.
- [90] M. Doucet and G. M. Clore. Global jumping and domain-specific intersegment transfer between DNA cognate sites of the multidomain transcription factor Oct-1. *Proceedings of the National Academy of Sciences*, 105(37):13871–13876, September 2008.
- [91] S. E. Halford, A. J. Welsh, and M. D. Szczelkun. Enzyme-mediated DNA looping. *Annual Review of Biophysics and Biomolecular Structure*, 33:1–24, 2004.

- [92] L. Zandarashvili, A. Esadze, D. Vuzman, C. A. Kemme, Y. Levy, and J. Iwahara. Balancing between affinity and speed in target DNA search by zinc-finger proteins via modulation of dynamic conformational ensemble. *Proceedings of the National Academy of Sciences*, 112(37):E5142–E5149, September 2015.
- [93] M. V. Sukhanova, S. Abrakhi, V. Joshi, D. Pastre, M. M. Kutuzov, R. O. Anarbaev, P. A. Curmi, L. Hamon, and O. I. Lavrik. Single molecule detection of PARP1 and PARP2 interaction with DNA strand breaks and their poly(ADP-ribosyl)ation using high-resolution AFM imaging. *Nucleic Acids Research*, 44(6):e60–e60, April 2016.
- [94] J. Rudolph, J. Mahadevan, P. Dyer, and K. Luger. Poly(ADP-ribose) polymerase 1 searches DNA via a ‘monkey bar’ mechanism. *eLife*, 7:e37818, August 2018.
- [95] J. Mahadevan, J. Rudolph, A. Jha, J. W. Tay, J. Dragavon, E. M. Grumstrup, and K. Luger. Q-FADD: A mechanistic approach for modeling the accumulation of proteins at sites of DNA damage by free diffusion. *bioRxiv*, page 373043, July 2018.
- [96] M. Feric, N. Vaidya, T. S. Harmon, D. M. Mitrea, L. Zhu, T. M. Richardson, R. W. Krivacki, R. V. Pappu, and C. P. Brangwynne. Coexisting Liquid Phases Underlie Nucleolar Subcompartments. *Cell*, 165(7):1686–1697, June 2016.
- [97] N. Shiina. Liquid- and solid-like RNA granules form through specific scaffold proteins and combine into biphasic granules. *Journal of Biological Chemistry*, 294(10):3532–3548, August 2019.
- [98] A. E. Posey, A. S. Holehouse, and R. V. Pappu. Chapter One - Phase Separation of Intrinsically Disordered Proteins. In E. Rhoades, editor, *Methods in Enzymology*, volume 611 of *Intrinsically Disordered Proteins*, pages 1–30. Academic Press, January 2018.
- [99] J. Wang, J.-M. Choi, A. S. Holehouse, H. O. Lee, X. Zhang, M. Jahnel, S. Maharana, R. Lemaitre, A. Pozniakovsky, D. Drechsel, I. Poser, R. V. Pappu, S. Alberti, and A. A. Hyman. A Molecular Grammar Governing the Driving Forces for Phase Separation of Prion-like RNA Binding Proteins. *Cell*, 174(3):688–699.e16, July 2018.
- [100] A. Catalano and D. H. O’Day. Evidence for nucleolar subcompartments in Dictyostelium. *Biochemical and Biophysical Research Communications*, 456(4):901–907, January 2015.
- [101] D. H. O’Day. Proteins of the Nucleolus of Dictyostelium discoideum: Nucleolar Compartmentalization, Targeting Sequences, Protein Translocations and Binding Partners. *Cells*, 8(2):167, February 2019.
- [102] S. Jain, J. R. Wheeler, R. W. Walters, A. Agrawal, A. Barsic, and R. Parker. ATPase-Modulated Stress Granules Contain a Diverse Proteome and Substructure. *Cell*, 164(3):487–498, January 2016.
- [103] L. Ristroph, A. J. Bergou, G. J. Berman, J. Guckenheimer, Z. J. Wang, and I. Cohen. Dynamics, Control, and Stabilization of Turning Flight in Fruit Flies. In S. Childress, A. Hosoi, W. W. Schultz, and J. Wang, editors, *Natural Locomotion in Fluids and on Surfaces*, The IMA Volumes in Mathematics and Its Applications, pages 83–99. Springer New York, 2012.

- [104] A. C. Noel and D. L. Hu. Cats use hollow papillae to wick saliva into fur. *Proceedings of the National Academy of Sciences*, 115(49):12377–12382, December 2018.
- [105] S. J. Gerbode, J. R. Puzey, A. G. McCormick, and L. Mahadevan. How the Cucumber Tendril Coils and Overwinds. *Science*, 337(6098):1087–1091, August 2012.
- [106] H. B. Schmidt and D. Görlich. Nup98 FG domains from diverse species spontaneously phase-separate into particles with nuclear pore-like permselectivity. *eLife*, 4:e04251, January 2015.
- [107] S. Milles, K. Huy Bui, C. Koehler, M. Eltsov, M. Beck, and E. A. Lemke. Facilitated aggregation of FG nucleoporins under molecular crowding conditions. *EMBO Reports*, 14(2):178–183, February 2013.
- [108] T. R. Jahn and S. E. Radford. Folding versus aggregation: Polypeptide conformations on competing pathways. *Archives of Biochemistry and Biophysics*, 469(1):100–117, January 2008.
- [109] L. Breydo, K. D. Reddy, A. Piai, I. C. Felli, R. Pierattelli, and V. N. Uversky. The crowd you're in with: Effects of different types of crowding agents on protein aggregation. *Biochimica et Biophysica Acta (BBA) - Proteins and Proteomics*, 1844(2):346–357, February 2014.
- [110] L. Breydo, A. E. Sales, T. Frege, M. C. Howell, B. Y. Zaslavsky, and V. N. Uversky. Effects of Polymer Hydrophobicity on Protein Structure and Aggregation Kinetics in Crowded Milieu. *Biochemistry*, 54(19):2957–2966, May 2015.
- [111] C. F. Lee, S. Bird, M. Shaw, L. Jean, and D. J. Vaux. Combined Effects of Agitation, Macromolecular Crowding, and Interfaces on Amyloidogenesis. *Journal of Biological Chemistry*, 287(45):38006–38019, February 2012.
- [112] A. Magno, A. Caflisch, and R. Pellarin. Crowding Effects on Amyloid Aggregation Kinetics. *The Journal of Physical Chemistry Letters*, 1(20):3027–3032, October 2010.
- [113] M. Sleutel, A. E. S. Van Driessche, W. Pan, E. K. Reichel, D. Maes, and P. G. Vekilov. Does Solution Viscosity Scale the Rate of Aggregation of Folded Proteins? *The Journal of Physical Chemistry Letters*, 3(10):1258–1263, May 2012.
- [114] S. Saha, A. Sharma, and S. Deep. Differential influence of additives on the various stages of insulin aggregation. *RSC Advances*, 6(34):28640–28652, 2016.
- [115] D. S. W. Protter, B. S. Rao, B. Van Treeck, Y. Lin, L. Mizoue, M. K. Rosen, and R. Parker. Intrinsically Disordered Regions Can Contribute Promiscuous Interactions to RNP Granule Assembly. *Cell Reports*, 22(6):1401–1412, February 2018.
- [116] M. M. Picken and G. A. Herrera. Thioflavin T Stain: An Easier and More Sensitive Method for Amyloid Detection. In M. M. P. M. FASN, A. D. M.D, and G. A. H. M.D, editors, *Amyloid and Related Disorders*, Current Clinical Pathology, pages 187–189. Humana Press, 2012.
- [117] R. Khurana, C. Coleman, C. Ionescu-Zanetti, S. A. Carter, V. Krishna, R. K. Grover, R. Roy, and S. Singh. Mechanism of thioflavin T binding to amyloid fibrils. *Journal of Structural Biology*, 151(3):229–238, September 2005.

- [118] M. Groenning. Binding mode of Thioflavin T and other molecular probes in the context of amyloid fibrils—current status. *Journal of Chemical Biology*, 3(1):1–18, August 2009.
- [119] A. N. Murray, F. L. Palhano, J. Bieschke, and J. W. Kelly. Surface adsorption considerations when working with amyloid fibrils in multiwell plates and Eppendorf tubes. *Protein Science*, 22(11):1531–1541, November 2013.
- [120] A. I. Sulatskaya, A. A. Maskevich, I. M. Kuznetsova, V. N. Uversky, and K. K. Turoverov. Fluorescence Quantum Yield of Thioflavin T in Rigid Isotropic Solution and Incorporated into the Amyloid Fibrils. *PLoS ONE*, 5(10), 2010.
- [121] L. Giehm and D. E. Otzen. Strategies to increase the reproducibility of protein fibrillization in plate reader assays. *Analytical Biochemistry*, 400(2):270–281, May 2010.
- [122] P. Arosio, T. P. J. Knowles, and S. Linse. On the lag phase in amyloid fibril formation. *Physical Chemistry Chemical Physics*, 17(12):7606–7618, March 2015.
- [123] L. A. Munishkina, E. M. Cooper, V. N. Uversky, and A. L. Fink. The effect of macromolecular crowding on protein aggregation and amyloid fibril formation. *Journal of Molecular Recognition*, 17(5):456–464, September 2004.
- [124] S. Prahl. Phenylalanine. <https://omlc.org/spectra/PhotochemCAD/html/073.html>, 1995.
- [125] A. S. Ladokhin. Fluorescence Spectroscopy in Peptide and Protein Analysis. In R. A. Meyers, editor, *Encyclopedia of Analytical Chemistry*, page a1611. John Wiley & Sons, Ltd, Chichester, UK, October 2000.
- [126] L. Serrano-Andrés and B. O. Roos. Theoretical Study of the Absorption and Emission Spectra of Indole in the Gas Phase and in a Solvent. *Journal of the American Chemical Society*, 118(1):185–195, January 1996.
- [127] J. Taylor. *An Introduction to Error Analysis*. University Science Books, 2nd edition, 1997.
- [128] H. Reich. 8-TECH-1 Relaxation in NMR Spectroscopy. <https://www.chem.wisc.edu/areas/reich/nmr/08-tech-01-relax.htm>, 2018. University of Wisconsin.
- [129] E. Pion, G. M. Ullmann, J.-C. Amé, D. Gérard, G. de Murcia, and E. Bombarda. DNA-Induced Dimerization of Poly(ADP-ribose) Polymerase-1 Triggers Its Activation. *Biochemistry*, 44(44):14670–14681, November 2005.
- [130] M. Altmeyer, S. Messner, P. O. Hassa, M. Fey, and M. O. Hottiger. Molecular mechanism of poly(ADP-ribosylation) by PARP1 and identification of lysine residues as ADP-ribose acceptor sites. *Nucleic Acids Research*, 37(11):3723–3738, June 2009.
- [131] T. Nozaki, R. Imai, M. Tanbo, R. Nagashima, S. Tamura, T. Tani, Y. Joti, M. Tomita, K. Hibino, M. T. Kanemaki, K. S. Wendt, Y. Okada, T. Nagai, and K. Maeshima. Dynamic Organization of Chromatin Domains Revealed by Super-Resolution Live-Cell Imaging. *Molecular Cell*, 67(2):282–293.e7, July 2017.
- [132] K. Maeshima, S. Ide, K. Hibino, and M. Sasai. Liquid-like behavior of chromatin. *Current Opinion in Genetics & Development*, 37:36–45, April 2016.